

A CATALOGUE OF ROTATION AND ACTIVITY IN EARLY-M STARS

ANSGAR REINERS AND NANDAN JOSHI

Institut für Astrophysik Göttingen, Physik Fakultät, Friedrich-Hund-Platz 1, D-37077 Göttingen

AND

BERTRAND GOLDMAN

Max-Planck-Institut für Astronomy, Heidelberg

Draft version January 30, 2012

ABSTRACT

We present a catalogue of rotation and chromospheric activity in a sample of 334 M dwarfs of spectral types M0–M4.5 populating the parameter space around the boundary to full convection. We obtained high-resolution optical spectra for 206 targets and determined projected rotational velocity, $v \sin i$, and H α emission. The data are combined with measurements of $v \sin i$ in field stars of the same spectral type from the literature. Our sample adds 157 new rotation measurements to the existing literature and almost doubles the sample of available $v \sin i$. The final sample provides a statistically meaningful picture of rotation and activity at the transition to full convection in the solar neighborhood. We confirm the steep rise in the fraction of active stars at the transition to full convection known from earlier work. In addition, we see a clear rise in rotational velocity in the same stars. In very few stars, no chromospheric activity but a detection of rotational broadening was reported. We argue that all of them are probably spurious detections; we conclude that in our sample all significantly rotating stars are active, and all active stars are significantly rotating. The rotation-activity relation is valid in partially and in fully convective stars. Thus, we do not observe any evidence for a transition from a rotationally dominated dynamo in partially convective stars to a rotation-independent turbulent dynamo in fully convective stars; turbulent dynamos in fully convective stars of spectral types around M4 are still driven by rotation. Finally, we compare projected rotational velocities of 33 stars to rotational periods derived from photometry in the literature and determine inclinations for a few of them.

Keywords: stars: M-stars – stars: activity – stars: rotation

1. INTRODUCTION

M-dwarfs constitute the majority of stars in the solar neighborhood. They are intrinsically faint because they are cooler and smaller than all other stars, and their physical properties span more than a factor of five in mass and radius from the coolest late-M-type stars and young brown dwarfs with less than a tenth of solar mass to the most massive M dwarfs with more than half a solar mass. Because of their faintness, detailed spectroscopic investigation is more observationally demanding than the analysis of brighter objects, but the sheer number of M stars renders them an excellent statistical sample for understanding properties of stellar physics and evolution. Many M dwarfs show substantial magnetic activity resulting in chromospheric and coronal heating, observed in various indicators across the whole stellar spectrum. It is often argued that M dwarfs are places of violent energy outbursts unsuitable for the existence of life. However, a large fraction of M dwarfs show little signs of magnetic activity, and M dwarfs have become a prime target for the search for Earth-like extrasolar planets.

The spectral type regime of early- to mid-type main sequence M stars coincides with the mass regime where the transition from partial convection to full convection occurs (Chabrier & Baraffe 1997). Partially convective stars, or solar-type stars, are believed to generate at least parts of their magnetic fields through a global dynamo re-

siding at the interface between the radiative core and the convective envelope. Rotational shear at this interface can amplify magnetic fields and sustain a cyclic magnetic dynamo (Parker 1993; Ossendrijver 2003). Field lines end up rising to the surface of the star and become visible in the form of starspots. Rotation, therefore, is the main driving force behind chromospheric and coronal activity. However, at $M \sim 0.35 M_{\odot}$ stars are believed to become fully convective and no interface layer exists anymore in their interior. The stars also suffer significant structural changes leading to dramatic differences in mass and radius while effective temperature (spectral type) only changes little. Therefore, radius and mass are strongly related to spectral subtype around the boundary to complete convection, which can explain the observed change in braking efficiency and activity lifetimes in this mass regime (Reiners & Mohanty 2011).

Despite the changes in stellar structure, strong magnetic activity also appears in very-low mass stars that are fully convective (Hawley et al. 1996; West et al. 2004). Observations of magnetically sensitive molecular lines (Reiners & Basri 2007; Shulyak et al. 2011), Zeeman Doppler imaging of M-stars (Donati et al. 2008; Morin et al. 2008) as well as numerical simulations of magnetic field generation in fully convective stars (Browning 2008) agree that strong magnetic fields exist across the full range of M-type dwarfs.

Rotation plays a crucial role in all scenarios of magnetic field generation. Observations of activity in

solar-type stars show a direct connection between rotation and activity, the so-called rotation-activity relation (Noyes et al. 1984; Delfosse et al. 1998; Pizzolato et al. 2003). Activity grows stronger with increasing rotational velocity and saturates at a threshold velocity that depends on the mass of the star (Pizzolato et al. 2003). The Rossby number $Ro = P/\tau_{\text{conv}}$, with P the rotation period and τ_{conv} the convective overturn time, is often used as a unifying scale of activity; activity saturates around $Ro = 0.1$. A saturation-type rotation-activity relation in M dwarfs is observed for late-M spectral types (later than M5; Mohanty & Basri 2003; Reiners & Basri 2010), and less well studied also in early-M type stars (Delfosse et al. 1998; Reiners & Basri 2007).

In this paper, we concentrate on early- to mid-M dwarfs including the transition from partial to complete convection. We include in our catalogue only stars of spectral type M0–M4.5. We took new observations that we combine with data from the literature. Our sample selection is explained in Section 2, analysis methods are described in Section 4 and discussed in Section 5.

2. OBSERVATIONS AND DATA REDUCTION

2.1. *New observations*

The goal of our project is to construct a statistically meaningful, yet neither complete nor unbiased, sample of early-M field dwarf spectra. Literature available at the time of observations containing considerable samples of high spectral-resolution analysis of field-M dwarf rotation velocities were Marcy & Chen (1992) and Delfosse et al. (1998). During the course of our project, Jenkins et al. (2009) and Browning et al. (2010) added more stars to this list, and a few other rotational velocities were presented in Reiners (2007) and Reiners & Basri (2007). We did not exclude young or halo stars from the sample in order to achieve a representative picture of the stars in the solar neighborhood.

Observations for this project were carried out at the spectrographs FOCES (CAHA, Calar Alto) in 2005, and FEROS (ESO, La Silla) in 2006 using time allocated through the the Max-Planck Institute for Astronomy (MPIA) at both observatories. In total, we have obtained spectra of 239 M0–M4.5 stars.

2.2. *Data reduction*

The FOCES echelle spectrograph at the 2.2m Telescope at CAHA, Calar Alto, was operated at spectral resolving power of approximately 40,000. Observations carried out with FEROS at the ESO/MPG 2.2m telescope at La Silla have a spectral resolution of approximately 48,000. Typical exposure times are between a few minutes and one hour per star for FEROS and up to two hours with FOCES. Individual exposures are always shorter than 30 min to avoid crowding with cosmic rays. The resulting signal-to-noise ratios are typically around 50, further analysis uncertainties are discussed in Section 4.

Data reduction followed standard procedures including bias subtraction, flat fielding, and wavelength calibration provided by ThAr or ThArNe lamps. For the FEROS spectra, reduction was done with the dedicated pipeline based on the MIDAS context, the FEROS Data Reduction System (DRS).

FOCES data was reduced using standard reduction procedures implemented in ESO-MIDAS. To avoid over- or underexposure for different échelle orders, three flat fields were taken with different exposure times, which is the usual procedure for FOCES data reduction. Orders were grouped in three sets each corresponding to different flat field exposure times, longest time corresponding to red and shortest time to blue regions in the spectrum. All three flat fields were merged to create a master flat field. The raw object spectra were freed from cosmic ray contamination and, after bias subtraction, flat-fielded with the master flat field. The wavelength scale was calibrated for each night using ThAr lamp calibrations. Scattered light was removed using a standard background subtraction routine in ESO-MIDAS. Since FOCES is a fiber-fed spectrograph, the object spectra were first extracted and then divided by the order-extracted master flat field.

3. THE CATALOGUE

In order to provide a comprehensive collection of currently available information on rotation and activity in early-M dwarfs, we created a catalogue of results from high-resolution spectra merging our results with catalogues published earlier and available in the literature. We tried to select work that used data of quality similar to ours and that were not selected according to physical parameters of the targets, i.e., we considered only work collecting data from selections of early-M field dwarfs. We limited our study to literature values of the objects in the same spectral range, M0.0–M4.5. Catalogues of this kind are Marcy & Chen (1992), Delfosse et al. (1998), Reiners (2007), Reiners & Basri (2007), Jenkins et al. (2009), and Browning et al. (2010). From Jenkins et al. (2009), we used only their own observations given in their Table 1 since the collection in their Table 3 is rather inhomogeneous and contains work focusing on young stars. We did not include results from the SACY sample (Torres et al. 2006) either since we focus on nearby field stars while the SACY targets form a specifically selected sample of young stars. All work considered provide information on $v \sin i$, but unfortunately quantitative information on H α emission is not available in all cases.

The distribution of stars as a function of spectral type is shown in Fig. 1. In this sample, known spectroscopic binaries are already removed (Section 4.3). In total, the sample consists of 334 M dwarfs of spectral types M0.0–M4.5. Spectra of 206 targets were taken during the course of this project, several of them were already available in the literature. Our observations add 157 new measurements of $v \sin i$ to the full catalogue.

The distribution of stars in our sample does not follow the distribution of stars in the solar neighborhood; in comparison to the distribution of M dwarfs, early-type stars are overrepresented in our sample. We can compare the distribution of stars in our sample to the mass function in the field reported by Bochanski et al. (2010). We use their system mass function parametrization in the lognormal form. In order to compare our distribution of spectral types to the mass function, we determine the mass of each spectral type bin and calculate the expected number of stars per bin. We assume the relation between spectral type and effective temperature according to the relation given in Kenyon & Hartmann (1995) and derive mass from temperature following the models

at 1 Gyr given in Baraffe et al. (1998). For simplicity, we assume constant bin sizes in mass for our spectral type bins, which is a reasonable approximation in our spectral type regime. For each spectral bin, we derive its range in $\log M$ and determine the number of stars within a 12 pc volume as expected from the mass function given in Bochanski et al. (2010). The result is shown as blue circles in Fig. 1. A volume-complete sample would include more mid-M stars per spectral bin than early-M stars. If our sample in each bin only contained the nearest stars, our sample would cover the volume out to ≈ 19 pc for M0 stars and slightly less than 12 pc for M4.5 stars. Although our sample cannot be considered complete out to any given volume, this shows how representative the sample is for the local Galaxy for the different stars contained; with respect to the local mass distribution of stars, early-M stars are overrepresented with respect to mid-M stars.

Our sample probes the local population of M stars. The sample of early-type stars is drawn from a population that extends up to two times further than our mid-M type stars. Since we do not expect significant differences in the properties of rotation and activity as a function of distance (between 10 and 20 pc), we do not expect that this influences the results respective to a volume-complete local sample. In any case, our results can be interpreted as representative for typical magnitude-limited surveys (as for example planet hunting missions will be).

3.1. $v \sin i$

Although the methodologies determining $v \sin i$ employed in the different studies are basically identical, there are some differences in their implementation. The basic idea is to compare the spectrum of a known, slowly rotating star (the template spectrum) with a spectrum of the science target in which the value of $v \sin i$ is to be determined. The template spectrum is convolved with rotational broadening profiles according to a set of different velocities using the scheme described in Gray (2005).

There are in principle two methods used to determine $v \sin i$. The first method is to directly compare a chosen set of individual spectral lines to artificially broadened template spectra. The value of $v \sin i$ is the one providing the best fit. This method is prone to systematic uncertainties induced by a mismatch between the template and science objects' spectra. The line profiles for comparison must be selected very carefully and systematic differences may occur if different sets of lines are used. This method determining $v \sin i$ was employed by Marcy & Chen (1992), Reiners (2007), Reiners & Basri (2007), and Jenkins et al. (2009). While Marcy & Chen (1992) and Jenkins et al. (2009) used atomic lines at optical wavelength ranges where blending is a serious issue, Reiners (2007) and Reiners & Basri (2007) employed lines of molecular FeH that are relatively free of blends and embedded in a rather well defined continuum.

The second method to derive values of $v \sin i$ is the so-called cross-correlation technique (Tonry & Davis 1979; Basri et al. 2000). Here, a slowly rotating template star is identified and its spectrum is cross-correlated with a series of the same template spectrum that is artificially broadened according to different rotational velocities. The widths of the correlation functions provide a calibrated measure of the value of $v \sin i$. Then, the tar-

get spectrum is cross-correlated with the non-broadened template spectrum and the width of the resulting correlation peak is converted into $v \sin i$ according to the calibration. Spectra are usually divided into several sections (e.g., spectral orders), and cross-correlation functions of individual orders may be averaged, or the median of individually derived $v \sin i$ values from different orders can be used. The latter procedure may also provide an estimate of the uncertainty. This cross-correlation method was employed in the analysis (see Section 4.2) of our new observations and in the work of Delfosse et al. (1998) and Browning et al. (2010).

3.2. Chromospheric activity

We collected measurements of projected rotational velocities from the literature. Unfortunately, not all literature also provide activity measurements together with rotation, or they provide only information on whether H α emission is detected or not, but not the value of equivalent width.

Delfosse et al. (1998) and Browning et al. (2010) include values of $\log L_{H\alpha}/L_{bol}$ in their tables, and we included their results in our catalogue. Marcy & Chen (1992) do not provide information on H α emission. Jenkins et al. (2009) provide only information on whether H α is detected, and whether they find H α in absorption in their spectra. If no H α was detected at all, we calculate upper limits for the stars assuming similar detection thresholds as for our data (see Section 4.1) because the data quality is similar. In cases where Jenkins et al. (2009) found H α in absorption, we treated these stars as inactive but mark them in our table. Although the existence of H α in absorption may be an indicator of weak activity (Cram & Mullan 1979), we classified these stars as inactive because all other work only considers H α emission as indicator for activity. In those cases where Jenkins et al. (2009) detected H α in emission, we do not provide any value in our table. The stars can easily be identified in the catalogue as those stars from Jenkins et al. (2009) that have no value of $\log L_{H\alpha}/L_{bol}$ in our catalogue.

Normalized luminosities or upper limits of it are available for 244 stars (73 % of our total sample of 334).

4. ANALYSIS

Normalized H α luminosity was calculated for our new spectra as a proxy for chromospheric activity, and projected rotational velocity was determined using the cross-correlation method.

4.1. Chromospheric activity

Chromospheric activity is measured from H α emission in our spectra. We estimated the continuum around H α taking the median of two different regions on either sides of H α line, namely: 6545–6559 Å and 6567–6580 Å. This value is used to normalize the spectra. We integrated the equivalent width of H α -emission in the spectral range 6552–6572 Å.

Many stars of our sample do not show significant line emission at H α . We conservatively estimated the detection limit of our spectra to 0.2 Å, which is consistent with the approach of Cayrel (1988) assuming a 3σ detection

limit with

$$\sigma_{\text{EqW}} = 1.5 \frac{\sqrt{\text{FWHM}_{\text{line}} \delta x_{\text{line}}}}{\text{S/N}} \quad (1)$$

and a typical SNR of 50. In this equation, $\text{FWHM}_{\text{line}}$ is the full width half maximum of the expected line and δx_{line} is the size of a resolution element.

Equivalent width is not a suitable indicator of stellar activity because the continuum flux is a steep function of effective temperature. We used PHOENIX model atmospheres (assuming $\log g = 5.0$ Hauschildt et al. 1999) to transform equivalent widths to $\text{H}\alpha$ flux, $F_{\text{H}\alpha}$, and we determine the flux ratio $F_{\text{H}\alpha}/F_{\text{bol}}$ using $F_{\text{bol}} = \sigma T^4$. Effective temperatures were derived from spectral type using the conversion given by Kenyon & Hartmann (1995). Finally, we use the identity $F_{\text{H}\alpha}/F_{\text{bol}} = L_{\text{H}\alpha}/L_{\text{bol}}$ to determine the ratio between $\text{H}\alpha$ and bolometric luminosity, i.e., normalized $\text{H}\alpha$ luminosity.

4.2. Rotation

In order to derive projected rotational velocities, $v \sin i$, from our spectra, we used the cross-correlation method as mentioned above. As a first step, the spectrum of a slowly rotating star was chosen as a template spectrum and artificially broadened according to a set of different velocities (Gray 2005). We chose velocities in the range $[1, 40] \text{ km s}^{-1}$, limb darkening was set to 0.6 (see Browning et al. 2010). The cross-correlation functions between the unbroadened template spectrum and the set of broadened spectra was calculated and the FWHM were determined as a function of $v \sin i$. To derive $v \sin i$ in a target spectrum, the cross-correlation function between the object spectrum and the template was calculated, an example is shown in Fig. 2. The FWHM is measured and converted into $v \sin i$ according to the calibration established from the broadened template spectra.

The two spectrographs used for our observations have somewhat different spectral resolving power. In order to avoid systematic differences between the two data sets, we employed different template spectra, i.e., one for each instrument. For the FOCES sample, we used a spectrum of Gl 2 as a template star, for the FEROS sample, Gl 84 was used. Both objects are of spectral type M2. We tried to use a few different template stars but found no systematic differences.

We estimated the detection limit for rotational broadening from our procedure to determine $v \sin i$. If we artificially broadened the spectra to simulate slow rotation ($v \sin i \lesssim 3 \text{ km s}^{-1}$), the FWHM of the cross-correlation profile only marginally differed from the auto-correlation function of the template. In our case, the spectral resolving power is not high enough to fully resolve the lines of slow rotators so that the threshold at which significant broadening becomes visible is determined by the spectral resolving power of the instrument. We find that from the FOCES spectra ($R = 40,000$) we can determine values of $v \sin i$ in excess of 4 km s^{-1} . For the FEROS spectra ($R = 48,000$), the detection limit is at $v \sin i = 3 \text{ km s}^{-1}$.

For the cross-correlation procedure, we use only selected spectral regions that are virtually free of telluric absorption and emission lines. We calculated correlation functions in 13 different spectral regions, each cov-

Table 1
Spectroscopic Binaries excluded from the Analysis

Name	$\alpha(J2000)$	$\delta(J2000)$	Spectral Type	Reference
Gl 1054A	03 07 56.0	-28 13 09	M 0.0	(1,2)
Gl 508A	13 19 45.5	+47 46 39	M 0.5	(1,2)
Gl 29.1	00 42 47.9	+35 32 54	M 1.0	(1,3)
Gl 616.2	16 17 05.4	+55 16 11	M 1.0	(1)
G 140-009	17 43 00.6	+05 47 21	M 1.0	(1)
Gl 804	20 44 21.9	+19 45 01	M 1.0	(1)
Steph 1806	20 40 56.4	-10 06 47	M 1.5	(1)
Gl 815A	21 00 04.9	+40 04 14	M 1.5	(1,2)
Gl 54	01 10 21.2	-67 26 54	M 2.5	(1)
Gl 268.3	07 16 19.7	+27 08 33	M 2.5	(1)
Gl 644A	16 55 28.1	-08 20 16	M 3.0	(1,4)
Gl 735	18 55 27.3	+08 24 09	M 3.0	(1)
Gl 206	05 32 14.6	+09 49 15	M 3.5	(1)
G 097-052	05 34 15.1	+10 19 15	M 3.5	(1)
Gl 263	07 04 17.2	-10 30 08	M 3.5	(1)
GJ 2069A	08 31 37.6	+19 23 39	M 3.5	(1,4)
Gl 375	09 58 33.3	-46 25 23	M 3.5	(1)
GJ 1212	17 13 40.6	-08 25 11	M 3.5	(1)
LP 476-207	05 01 58.7	+09 58 59	M 4.0	(1,4)
LHS 2887	14 17 03.2	+31 42 47	M 4.0	(1,4)
Gl 381	10 12 04.3	-02 41 00	M 2.5	(4)
GJ 1080	05 28 14.8	+02 58 23	M 3.0	(5)
Gl 487	12 49 03.1	+66 06 37	M 3.0	(4)
Gl 747(A)	19 07 42.1	+32 32 32	M 3.0	(4)
LHS 6158	08 58 56.1	+08 28 28	M 3.5	(4)
G 203-47	17 09 31.2	+43 40 54	M 3.5	(4)
Gl 661(A)	17 12 07.5	+45 40 09	M 3.5	(4)
Gl 896A ^a	23 31 51.8	+19 56 14	M 3.5	(4)
Gl 695BC	17 46 27.2	+27 43 07	M 3.5	(4)
GJ 3129	02 02 44.0	+13 34 33	M 4.5	(5)
Gl 268	07 10 07.8	+38 31 27	M 4.5	(2)
GJ 1103(A)	07 51 56.7	-00 00 08	M 4.5	(4)
LHS 3080	15 31 54.4	+28 51 08	M 4.5	(5)
GJ 1230A	18 41 09.3	+24 47 14	M 4.5	(4)
Gl 831(A)	21 31 17.8	-09 47 25	M 4.5	(4)

References. — (1) New Observations; (2) Gizis et al. (2002); (3) Browning et al. (2010); (4) Delfosse et al. (1998); (5) Jenkins et al. (2009).

^a Gl 896B is located less than 1 \AA from the A component. It has measured $v \sin i$ of 24.2 km s^{-1} in Mohanty & Basri (2003). It cannot be confirmed whether the estimates are for both components combined.

ering approximately 20 \AA . The spectral regions are not identical in the FEROS and FOCES samples, which is due to the different performances of the instruments and their coverage of échelle orders. The projected rotational velocity was calculated for each spectral region; the adopted final rotational velocity is the mean of the individual values. The standard deviation for stars with $v \sin i < 20 \text{ km s}^{-1}$ is typically below 1 km s^{-1} . Note that this value is much smaller than the detection limit because it is the typical scatter in $v \sin i$ between individual orders while the detection limit is the lowest value of $v \sin i$ at which rotation can be distinguished against other broadening agents like temperature and instrumental broadening. The uncertainty of our $v \sin i$ measurements also is not the same as the intra-order scatter, it is the accuracy at which we can distinguish rotation from other broadening agents; we estimate the final uncertainty to be $\sim 3 \text{ km s}^{-1}$ for slow rotators but not less than 10 % (see Reiners 2007; Reiners & Basri 2007).

4.3. Spectroscopic binaries

Complete information on binarity in stars is difficult to achieve. Binarity may be detected using high spatial res-

Table 2
Possible Spectroscopic Binaries Excluded from the
Analysis

Name	$\alpha(J2000)$	$\delta(J2000)$	Spectral Type
G 235-020	09 19 23.0	+62 03 18	M 0.0
Gl 341	09 21 40.2	-60 16 58	M 0.0
Gl 373	09 56 08.9	+62 47 21	M 0.0
GJ 1181A	13 55 02.8	-29 05 23	M 0.0
Gl 737A	18 57 30.6	-55 59 19	M 0.0
LTT 8848	22 05 51.3	-11 54 48	M 0.0
GJ 1135	10 41 08.9	-36 53 42	M 0.5
BPM 11774	18 50 25.7	-62 03 02	M 0.5
G 144-016	20 37 20.8	+21 56 54	M 0.5
Gl 207.1	05 33 44.8	+01 56 43	M 2.5
GJ 1136A	10 41 50.6	-36 37 53	M 2.5
LHS 221A	06 54 03.7	+60 52 24	M 3.0
Gl 352A	09 31 18.9	-13 29 18	M 3.0

olution imaging, but in many cases binary components are too close to each other and cannot be spatially resolved. In such a case, the observed spectrum consists of light from all components weighted according to their luminosity. If both components are similar in luminosity, both spectra appear in the spectrum with a separation according to the difference in radial velocities at the time of observation. For the search for spectroscopic binaries, the cross-correlation profile is very useful. Three cases can be distinguished: 1) The separation is larger than the typical line-width. In such a case, two systems of spectral lines are visible in the spectrum and the cross-correlation profile shows two separated maxima; 2) The separation is on the order of the typical line-width. Here, the cross-correlation function is broader than individual correlation maxima due to single stars. The profile may appear asymmetric depending on the luminosity difference of the components and their radial velocity difference. Fig. 3 shows a typical cross-correlation profile with significant asymmetry that is attributed to a spectroscopic binary; 3) The separation is marginally different from zero. The profile appears only slightly wider than the typical single profile and may be asymmetric.

If a system is a multiple system instead of a single star, the determination of rotation becomes meaningless unless individual components can be disentangled from each other. We found that 20 stars of our originally observed sample are spectroscopic binaries that could be unambiguously identified. The stars are listed in Table 1 and are not used for further analysis and the catalogue. For completeness, Table 1 also includes spectroscopic binaries of spectral types M0.0–M4.5 reported in the literature.

Our cross-correlation analysis revealed that 13 other stars have asymmetric cross-correlation profiles. The degree of asymmetry is small but justifies the assumption that the stars are no regular single objects. They may be spectroscopic binaries with long periods or observed at very similar radial velocities. We exclude these objects from our sample analysis. The marginal outliers are listed in Table 2, further observations at a different epoch may clarify whether these stars are in fact binaries.

5. RESULTS

Our catalogue of early- to mid-M dwarfs with measured rotational velocities together with information about activity is given in Table 6. Spectral types are taken from

Reid et al. (1995). Information on activity and rotation from our observations and the literature are given as explained in the foregoing sections.

5.1. Chromospheric activity

In Fig. 4, we show normalized $H\alpha$ activity as a function of spectral type. In total, our catalogue contains 244 stars with $H\alpha$ measurements, 95 of them (39%) are active. It is well established that activity lifetimes are substantially longer at later spectral types (e.g., Hawley et al. 1996; Gizis et al. 2002; Silvestri et al. 2005; West et al. 2008). Stars on the cool side of the boundary to complete convection appear active much longer, leading to the observation that many more fully convective stars show activity. On the hot side of that boundary, where stars are believed to still harbor a tachocline and hence may drive a Sun-like large-scale dynamo, only very few active stars are known in the field. Virtually all active early-M stars are members of young associations, several examples can be found in Torres et al. (2006). Partially convective early-M stars in the field, however, that are believed to be older, in general do not possess significant activity. Within the literature concerned for our catalogue, there is no early-M type star ($<M3$) with significant activity that is not a known member of a young association. Thus, any single early-M type active star is probably young, which means not older than a few 100 Myr. In fully convective stars, however, activity can persist for several Gyr and we expect to find many more active stars of spectral type M3 and later. Note that rapid rotation and hence enhanced activity may be maintained in tidally locked binaries.

The total catalogue contains seven out of 129 (5%) early-M type stars exhibiting significant activity as $H\alpha$ emission. In contrast, 47 out of 115 (41%) stars between M3 and M4.5 are active. The fraction of active stars as function of spectral type is shown in Fig. 5, it is in general higher than reported in West et al. (2008) from the SDSS sample, which is consistent with our sample being younger than the sample used there (observed away from the Galactic plane), and our results are consistent with earlier work on the activity fraction of field stars (e.g., Hawley et al. 1996; Gizis et al. 2002; Silvestri et al. 2005). The general trend, however, is very well reproduced. A relatively sharp transition from a low activity fraction smaller than 10% to a significant fraction above 50% occurs around spectral type M3. From activity information alone, we cannot determine the reason for this dramatic increase. West et al. (2008) speculate that longer activity lifetimes may be explained by a transition from a rotationally-dependent solar-like dynamo to a rotationally-independent turbulent dynamo in which magnetic fields can survive much longer even if the stars are rotating slower. We come back to this point when we discuss the rotation of these stars in Sect. 5.3.

5.2. Active early-M dwarfs

Field stars are believed to be relatively old (\sim Gyr) and early-M dwarfs ($<M3$) are in general not observed to be active in the field. In our survey, we found or confirmed activity in seven out of 129 (5%) early-M targets with $H\alpha$ measurements. The reason for their activity is probably youth since it is known that early-M dwarfs can

Table 3
Active early-M stars

Name	Spectral type	$\log(L_{H\alpha}/L_{bol})$	$v \sin i$ [km/s ⁻¹]
GJ 182	M0.0	-4.11	10.4
GJ 494	M0.5	-3.80	9.7
Steph 546A	M1.5	-3.89	5.3
Wo 9520	M1.5	-3.92	6.5
GJ 2036A	M2.0	-3.45	44.3
GJ 358	M2.0	-4.44	< 3.0
GJ 569A	M2.0	-4.30	< 2.5

be very active at young ages. Young stars are rotating much more rapidly and therefore can generate sufficient magnetism to generate magnetic activity (Pizzolato et al. 2003). A potential reason why a field early-M dwarf can generate activity is prevention of angular momentum loss because of binarity. Another explanation is that the star is indeed young and entered our survey because it is relatively nearby compared to other young objects. Finally, some stars may be mis-classified in spectral type so that they are actually within the regime of M3 or later.

The seven active early-M dwarfs found in our survey are presented in Table 3. Spectral types are between M0 and M2, mis-classification may be an issue for the latest targets but is unlikely for all of them. Some of the stars have companions but we did not find evidence for binarity in any of the stars that would sufficiently influence the rotation of the star on Gyr-timescales. Most of the objects are probably young objects in the solar neighborhood. We discuss the seven stars individually in the following:

GJ 182 is a young star known as V1005 Ori. The star is contained in the SACY sample (Torres et al. 2006; da Silva et al. 2009) and classified as a member of the β Pictoris young association (10 Myr). It shows substantial activity ($\log L_{H\alpha}/L_{bol} = -4.11$) and rapid rotation ($v \sin i = 10.4 \text{ km s}^{-1}$).

GJ 494A has a companion of spectral type M7 at a separation of $0.475''$ (Beuzit et al. 2004), and a planetary candidate companion of spectral type T8-9 at $102''$ (Goldman et al. 2010). The secondary component is too faint to influence the rotational profile and our measurement of $v \sin i$ is most likely the one of the M0.5 primary alone. Beuzit et al. (2004) determine $v \sin i = 9.6 \text{ km s}^{-1}$ consistent with our observations. They conclude that the object is not a short-period locked binary but a rapidly rotating, young early-M star (see also Burgasser et al. 2010; Burningham et al. 2011).

Steph 546A (GJ 3331A) also is contained in the SACY survey under the name BD 21 1074A. It is classified as a member of the β Pic association (da Silva et al. 2009) and has a companion pair, BD 21 1074BC.

Wo 9520 (GJ 9520) was observed by Daemgen et al. (2007) using the Altair AO System at Gemini North Observatory. No companion could be detected. Shkolnik et al. (2009) observed the star at two different epochs and found no evidence for RV variability providing evidence that Wo 9520 is not a binary system. Shkolnik et al. (2009) estimate an age of 15 – 150 Myrs.

GJ 2036A (CD-56 1032A) is part of a binary system with two active components. The system is classified as a member of the AB Doradus young association (70 Myrs) by da Silva et al. (2009).

GJ 358 is identified as a possible member of the Carina-Near Stream by Zuckerman et al. (2006), which would imply an age of ~ 200 Myr.

GJ 569A is accompanied by the brown-dwarf brown-dwarf pair GJ 569Bab (Simon et al. 2006; Femenía et al. 2011) for that orbital parameters are well determined. Comparison of the colors of GJ 569Bab to theoretical isochrones and color mass diagrams suggest an age of 100–125 Myr, which is probably the same as for GJ 569A. The orbital inclination of GJ 569Bab is $(32.4 \pm 1.3)^\circ$ ($\sin i = 0.54$; Simon et al. 2006).

Five out of the seven active early-M stars show detectable rotation in $v \sin i$. The two other stars, in which no rotation was detected, GJ 358 and GJ 569A, may be observed under high inclination. Both stars show relatively low activity compared to the other stars in Table 3 so that their equatorial velocities are probably comparably low, i.e. only a few km s^{-1} . Inclination angles below $\sim 60^\circ$ may be sufficient to push $v \sin i$ below the detection limit, which renders this scenario rather likely. In particular, this is consistent with the assumption of spin-orbit alignment in the GJ 569 multiple system ($i \approx 30^\circ$).

For each of the seven active early-M stars, Kiraga & Stepien (2007) provide a photometric period. This may be a hint that spot configurations in active early-M dwarfs are rather stable at least after a few 10 Myr. However, periodicity may not in all cases be due to rotation. We discuss photometric periods in Sect. 6.

5.3. Rotation

We provide measurements or upper limits of the projected rotational velocity, $v \sin i$, for all 334 stars of our catalogue. As explained above, detection thresholds for our new measurements with the FOCES and FEROS spectrographs are estimated at 4 and 3 km s^{-1} , respectively, according to the spectrographs' different resolving power. Detection limits of the collected data from the literature also vary. Browning et al. (2010) estimate a detection limit of $v \sin i_{lim} = 2.5 \text{ km s}^{-1}$ ($R = 45,000$ – $60,000$), Reiners & Basri (2007) use $v \sin i_{lim} = 3 \text{ km s}^{-1}$ ($R = 31,000$), and Reiners (2007) used extremely high-resolution data ($R \approx 200,000$) estimating $v \sin i_{lim} = 1 \text{ km s}^{-1}$. Furthermore, we adopt $v \sin i_{lim} = 3 \text{ km s}^{-1}$ for results from Marcy & Chen (1992, $R = 40,000$) and $v \sin i_{lim} = 2 \text{ km s}^{-1}$ for those from Delfosse et al. (1998, $R = 42,000$) as written in those publications. Jenkins et al. (2009) do not quote a general detection threshold in $v \sin i$. Using spectra at a spectral resolving power of $R = 37,000$, they determine individual upper limits as well as many detections at the $v \sin i = 3 \text{ km s}^{-1}$ level. We adopt these values as they are given in the original literature but show below that their detection threshold is likely higher, around $v \sin i_{lim} = 4 \text{ km s}^{-1}$.

Several stars are contained in more than one of the considered works. Individual measurements may differ because spectral appearance can change with chromospheric variability or different authors used differ-

ent spectral lines in their analysis that are sensitive to chromospheric activity. We provide a list of all stars with more than one $v \sin i$ measurement in Table 7. In general, all measurements from different data are consistent within the uncertainties, the only outliers are two measurements of $v \sin i$ in Gl 388 and Gl 873 by Delfosse et al. (1998). For the inactive stars Gl 369, G 244-047.01, and GJ 1119, rotational broadening is reported in one paper but not detected in one or more other works. These stars are probably rotating very slowly as we discuss below. Gl 388 (AD Leo), Gl 729 (V1216 Sgr), and Gl 873 (EV Lac) are very active stars for that different analyses report $v \sin i$ values close to the detection limits. These stars are probably rotating on the few km s^{-1} level.

For our catalogue, we adopted $v \sin i$ values according to the following strategy. Preference was given to the $v \sin i$ data from the work done with the highest spectral resolution. Highest priority was given to results Reiners (2007) because they are derived from the highest resolution spectra. Second highest priority is given to the results from Browning et al. (2010). If both are not available and several other works provided measurements of $v \sin i$, we chose to use the one from our new measurements. In Fig. 6, we show a comparison between $v \sin i$ measured in this work and data from the literature. For all stars, values are consistent within the uncertainties and detection limits.

Projected rotational velocities, $v \sin i$, for our catalogue are plotted as a function of spectral type in Fig. 7. The situation appears very similar to the one in Fig. 4 where activity was shown as a function of spectral type. Again, we see only a few early-M type stars with significant rotation (shown as open circles in Fig. 7). These stars are listed in Table 3 and discussed individually in Sect. 5.2. At later spectral types ($\geq M3$), significant rotation appears to be more frequent just as activity is more frequent in this spectral range. In total, 51 stars of our 334 stars (15%) show rotational broadening of $v \sin i \geq 3 \text{ km s}^{-1}$.

Fig. 8 shows the fraction of rapid rotators, i.e., stars with detected rotational broadening $v \sin i \geq 3 \text{ km s}^{-1}$, as a function of spectral type. The picture appears to be very similar to the fraction of active stars discussed above (Fig. 5). While among early-M type stars ($< M3$), the fraction of rapid rotators is below 5%, it rises rapidly to approximately 45% at spectral type M4.

5.4. Rotation-activity relation

After our discussions of activity and rotation in the sample catalogue, we now turn to the relation between the two across the spectral range M0.0–M4.5, i.e., from partially convective Sun-like stars to fully convective stars. The two distributions in Figs. 5 and 8 are strikingly similar. Within statistical uncertainties, the distributions of active and rapidly rotating stars are consistent with the assumption that active stars and rapid rotators are both drawn from the same underlying population. We tested the probability that both distribution are drawn from the same distribution following Kolmogorov-Smirnov statistics (Press et al. 1992). In numbers, the probability that the sample of active stars and the sample of rapidly rotating stars are drawn from independent distributions is lower than $4 \cdot 10^{-4}$. This means that

rotation and activity are highly correlated and that the active stars in our sample are likely the same stars as the rotating ones. While this does not prove a causal relation between rotation and activity, it provides evidence that both occurs in the same stars.

It is worth emphasising that evidence for a correlation between activity and rotation exists *over the entire sample* including both partially and fully convective stars. In other words, before we discuss the relation between rotation and activity on the basis of individual stars, the distribution of rotation and activity in M0–M4 stars already provides strong evidence for the validity of the rotation-activity connection across the boundary to complete convection.

We plot normalized $H\alpha$ luminosity, $\log L_{H\alpha}/L_{\text{bol}}$, against projected rotational velocity, $v \sin i$, in Fig. 9. In the figure, we further discriminate between partially convective stars ($< M3$) and likely fully convective stars ($M3$ and later). The boundary between the two groups is likely not sharp and spectral type uncertainties on the order of 0.5–1 spectral subtypes further softens the location of this transition. As a first result, we can confirm the rotation-activity relation in the sense that low activity ($\log L_{H\alpha}/L_{\text{bol}} < -4.5$) only occurs at slow rotation. There are a handful of inactive stars (stars with low activity) for that detections of rotational line broadening on the order of $4\text{--}5 \text{ km s}^{-1}$ is detected. We discuss these stars in Sect. 5.5. Furthermore, we can conclude that the correlation between rotation and activity is valid at both sides of the convection boundary, i.e., for both early- and later-M type stars (open and solid symbols in Fig. 9).

Active stars are found at virtually all rotation rates. In our sample, we found 48 very active stars with $\log L_{H\alpha}/L_{\text{bol}} > -4.5$. Among them, 33 stars are rapid rotators ($v \sin i > 3 \text{ km s}^{-1}$). This means that 15 out of 48 active stars (31%) have rotation velocities below our detection limit, or are observed under low inclination angles so that high rotation rates are not detected. In the latter scenario, the most active stars at low $v \sin i$ values are interpreted as stars observed under very low angles i . We can test the assumption whether a tight relation between rotation and activity is valid among all our sample stars. If so, all stars with very high $H\alpha$ emission, say $\log L_{H\alpha}/L_{\text{bol}} > -4.0$, would be rotating at approximately $v \sin i \gtrsim 5 \text{ km s}^{-1}$, which means that at a typical detection threshold of $v \sin i_{\text{lim}} = 3 \text{ km s}^{-1}$, inclination must be such that $\sin i < 0.6$ ($i < 37^\circ$). In our sample, 7 out of 36 (19%) stars with $\log L_{H\alpha}/L_{\text{bol}} > -4.0$ show no detectable rotation. In a sample of stars with randomly oriented rotation axes, a fraction of 19% will be observed at inclination angles smaller than 36° , i.e., $\sin i < 0.59$. Thus, we can conclude that the distribution of measurements in $v \sin i$ and activity is consistent with the assumption of a well-defined relation between rotation and activity that is spread out in Fig. 9 due to projection effects from observing the stars under statistically distributed orientations.

Active M stars are known to exhibit frequent flaring events that introduce substantial scatter in $\log L_{H\alpha}/L_{\text{bol}}$ and is difficult to quantify with just one observation. Kowalski et al. (2009) found that among a sample of 236 stars with flares, $\sim 3\%$ show no $H\alpha$ emission outside the flare. If we assume that inactive stars with occa-

Table 4

Inactive stars reported to be rapidly rotating. Stars marked with an asterisk show H α in absorption (Jenkins et al. 2009).

Name	Spectral type	$\log(L_{H\alpha}/L_{bol})$	$v \sin i$ [km s $^{-1}$]
GJ 3104	M3.0	< -4.90*	4.0
LHS 2651	M3.5	< -4.93	3.9
LHS 1785	M4.5	< -4.97	4.5
LHS 1857	M4.5	< -4.97	4.0
GJ 3542	M4.5	< -4.97	3.9
GJ 1134	M4.5	< -4.97*	4.1
G 121-028	M4.5	< -4.97*	3.8
GJ 1186	M4.5	< -4.97	3.9
Gl 585	M4.5	< -4.97*	3.1

References. — All $v \sin i$ values from Jenkins et al. (2009)

sional flaring are slow rotators, we can estimate that one star of our 33 slowly rotating flare stars is in fact an inactive, slow rotator. Furthermore, Hilton et al. (2010) determined the flare rates of stars at different spectral types, for stars of our sample the flare rates are $\leq 1\%$. Although it is not trivial to compare the flare rates from Hilton et al. (2010) to our sample because of the inhomogenous distribution of exposure times, we can exclude a significant influence of flaring on the occurrence of active stars for which no evidence of rotation could be detected.

In Fig. 9, we have distinguished between early-M type stars ($< M3$, open symbols) and later M stars (solid symbols) expecting the transition from partially to fully convective stars at this spectral range. The subsample of early-M dwarfs is defined by a number of inactive, slowly rotating stars (with several upper limits in $v \sin i$) and seven active stars, five of them with detected rotation. The early-M dwarfs exhibit a clear correlation between projected rotation rate and normalized H α activity; all stars with $v \sin i \approx 3 \text{ km s}^{-1}$ and above are active, and the stars with $v \sin i \geq 5 \text{ km s}^{-1}$ show higher activity than those at $v \sin i \approx 3 \text{ km s}^{-1}$. Interestingly, the scatter in activity in early-M stars at $v \sin i \geq 5 \text{ km s}^{-1}$ is much smaller than the scatter in mid-M stars in our sample. From our small sample, it is not possible to decide whether this is an intrinsic effect or due to the small number of rapidly rotating early-M stars, but it is consistent with the conclusion of Gizis et al. (2002) and Lee et al. (2010) that the H α variability is larger at later spectral types. In fully convective star, the scatter of H α activity is much larger than in early-M dwarfs, but as in early-M dwarfs all significantly rotating fully convective show significant H α activity. In summary, the saturation-type rotation-activity relation is intact until spectral type M4.5, while the scatter is perhaps growing larger in lower-mass stars that generally tend to be more active in our sample.

5.5. Rapidly rotating inactive stars

The relation between rotation and activity may not be valid in all individual cases. In general, rotation generates magnetic activity, but we may still find activity in some stars that are observed at low *projected* rotation rates, or even in stars that are slowly rotating but active for reasons we have not understood. On the other hand,

our assumption of magnetic dynamo operation triggered by rotation leads to the expectation that *all* rapidly rotating stars show significant values of magnetic activity. West & Basri (2009) reported the existence of three rapidly rotating but inactive stars at spectral types later than our sample (M6–M7). We searched for such stars in our sample of hotter M stars.

Table 4 lists nine stars in which no H α emission was found but a detection of rotational broadening was reported. All nine stars are from the catalogue of Jenkins et al. (2009), and all stars have values of $v \sin i$ between 3 and 4.5 km s^{-1} . Four of the nine stars are reported to show H α in absorption, which is evidence for very low but non-zero activity.

Regardless whether or not the stars with H α absorption are indeed weakly active, it is striking that all nine stars are found in the same work. Our catalogue contains 23 stars taken from Jenkins et al. (2009), nine of them show no activity in the presence of rotation. Among the 311 stars taken from other sources, not a single star shows similar properties. The spectral resolution of the data used by Jenkins et al. (2009) is $R = 37,000$. For such data, a detection limit between 3 and 5 km s^{-1} can be expected depending on SNR, that means at the same order as the measurements reported for the stars in Table 4. We argue that the absence of rapidly rotating inactive stars in the rest of our sample provides ample evidence that *all* rapid rotators $v \sin i \gtrsim 3 \text{ km s}^{-1}$ show measurable H α activity, and that the reported detections of rotation in inactive stars from Jenkins et al. (2009) are spurious and in fact upper limits to their real values of $v \sin i$. Our conclusion is that substantial chromospheric emission is a fundamental consequence of rapid rotation in M0–M4.5 stars.

6. COMPARISON TO PHOTOMETRIC PERIODS

Stellar line broadening provides information about the projected rotation velocity on the surface of a star. A more convenient and physically meaningful property is the rotation period of the star. Period P and projected surface velocity $v \sin i$ are related through

$$v \sin i = \frac{2\pi R \sin i}{P}, \quad (2)$$

with R the stellar radius. Measuring photometric periods in M dwarfs is notoriously difficult because of the high activity these stars reach even at relatively long periods. This means that spot lifetimes may be shorter than typical rotation periods. We collected photometric periods from Irwin et al. (2011) and Kiraga & Stepień (2007), the latter including reference to period measurements for Gl 411 (Noyes et al. 1984) and Gl 699 (Benedict et al. 1998). Furthermore, we consider periods collected in Messina et al. (2003), namely periods for Gl 410 (Fekel & Henry 2000) and Gl 735 (Alekseev 1998), and periods presented in Engle et al. (2009) including the period of Gl 873 from Contadakis (1995). We augment our sample of M0.0–M4.5 stars with three additional stars of spectral type M5, GJ 1057 and GJ 1156, for which rotational periods are reported by Irwin et al. (2011), and Gl 551 (period from Kiraga & Stepień 2007), and in which measurements of $v \sin i$ are available. From the period, we estimated the star’s surface veloc-

ity for which information on stellar radius is required. Irwin et al. (2011) provide radius estimates for their targets. For the stars in Kiraga & Stepień (2007, including Gl 411 and Gl 699), we adopted the stellar masses provided there and assumed that stellar radius in solar units has the same value as stellar mass expressed in solar units (i.e., for a star with $M = 0.5 M_{\odot}$ we assumed $R = 0.5 R_{\odot}$; see Demory et al. 2009). For the other stars we used the strategy of Kiraga & Stepień (2007), calculating mass from the V -band mass-luminosity relation in Delfosse et al. (2000) and assumed mass-radius identity as above.

The stars with rotational period measurements are shown in Table 5. For each star, we calculated the equatorial surface velocity, v_{eq} , derived from the period and compared it to the measured projected surface velocity $v \sin i$. The two velocities, v_{eq} and $v \sin i$, are compared in the left panel of Fig. 10. If period and surface velocity are consistent, the stars should populate the region close to the line of identity (drawn as solid line in Fig. 10). Stars observed under low inclination angles i are expected to fall below that line. Comparing the values v_{eq} and $v \sin i$, we find that several stars are far away from the line of unit slope. From the typical scatter in the mass-luminosity relation, uncertainties in parallax and photometric measurements, and the scatter in the mass-radius identity, we estimated that the final uncertainty in v_{eq} is typically much lower than 50 %, which translates into uncertainties in the inclination much lower than a factor of 2. Therefore, very low inclination angles (below $\sim 50^\circ$) are unlikely to be caused by uncertainties in measuring $v \sin i$ or the translation into v_{eq} .

Stars with $v \sin i < v_{\text{eq}}$ may be observed under small inclination angles, for these stars we plot inclination i as a function of rotation period in the lower right panel of Fig. 10. M-type stars with rotation periods on the order of $P = 10$ d and longer have surface rotation velocities below the typical detection limits of $v \sin i$ measurements. These stars are marked with downward arrows in Fig. 10. Although we cannot determine information about inclination for those stars, the non-detection of rotational broadening means that spectroscopic measurements are consistent with the reported photometric periods. For some stars, however, we find measurements of rotation velocities with $v \sin i > v_{\text{eq}}$. For all stars with $v \sin i > v_{\text{eq}}$ (including upper limits in $v \sin i$), we calculate the ratio between projected rotation velocities and photometrically derived surface velocity, $v \sin i / v_{\text{eq}}$, and plot this ratio in the upper right panel of Fig. 10. As expected, for very long periods, limited spectral resolving power leads to very large ratios.

The first conclusion from the comparison between photometric periods and projected rotation velocities is that both measurements are consistent for several stars with measured $v \sin i$ above the detection limit, and the majority of upper limits in $v \sin i$ are consistent with surface rotation velocities being below the spectroscopic detection limit. There are two groups of stars in which spectroscopic and photometric rotation rates are not consistent: (1) Among the stars with rotation periods shorter than 10 d, seven stars have inclination angles below $i = 60^\circ$ while eight stars have larger inclination angles but ratios of $v \sin i / v_{\text{eq}}$ not much larger than 1. The fraction of stars with $i < 60^\circ$ is 47 %, which is consis-

tent with the assumption of random orientation of the rotation axis (leading to an expected fraction of 50 % with $i < 60^\circ$). On the other hand, several stars have extremely small inclination angles, for example two stars have $i < 5^\circ$. The fraction of stars with such low an inclination angle in a sample of randomly oriented spin axes is only 0.4 %, yet 14 % of the stars in this subsample are found. Thus, the fraction of stars with very low inclination angles appears to be unrealistically low. (2) Three stars exist in our sample in which $v \sin i$ exceeds v_{eq} by a factor of 2 or higher (marked as red stars in Fig. 10). Here, spectroscopic and photometric measurements are clearly inconsistent.

Inconsistencies between spectroscopic and photometric measurements can have several reasons. First, a high frequency of stars observed under very small inclination angles could be due to an observational bias. Photometric periods are most likely to be detected in stars that show large brightness variations. If a star is observed pole-on, brightness variations caused by corotating spots are smaller than if the star is observed under high inclination. This results in a potential bias towards the detection of photometric periods in stars with large values of i . Thus, this bias results in a *lower* fraction of stars with very small i than expected from random distribution of rotation axes. Taking this bias into account, the existence of several stars with very small inclination angles is even more unlikely. Another potential source of error are incorrect period measurements. Period measurements from Irwin et al. (2011) are based on several hundred data points and show clear periodicity as demonstrated in that paper. The quality of other period reports is generally lower simply because of the exquisite data quality used in Irwin et al. (2011). For example, photometric data used for the Kiraga & Stepień (2007) periods are of much lower quality. Nevertheless, many periods reported in Kiraga & Stepień (2007) look rather convincing as demonstrated by the authors. In our sample, we identified five period measurements that are inconsistent with $v \sin i$ measurements possibly because of period misidentifications; Gl 431 and GJ 2036A have periods much lower than expected from $v \sin i$ ($v \sin i / v_{\text{eq}} \geq 2$), and Steph-546A, Wo 9520, and Gl 669A have extremely low inclination angles ($i < 15^\circ$). The periods for all these stars are from Kiraga & Stepień (2007), and visual inspection of their phase-folded lightcurves indeed shows that misidentification of these periods is likely. It is interesting to note that for GJ 2036A surface equatorial velocity and spectroscopic projected rotation velocity differ by exactly a factor of two. A photometric period of 1.6 d instead of 0.8 d would agree with the spectroscopic measurement. A potential reason for this difference may be that the 0.8 d period is an alias of a 1.6 d period.

A third potential reason for inconsistencies between spectroscopic and photometric measurements is an incorrect estimate of $v \sin i$. This is a likely explanation for one of our cases: GJ 1186 has $v \sin i = 3.9 \text{ km s}^{-1}$ exceeding v_{eq} by a factor of 40. Here, the phase-folded lightcurve presented by Irwin et al. (2011) looks very reasonable. The value of $v \sin i$ is from the catalogue of Jenkins et al. (2009) and similar to the values shown in Table 4 for which we argued that these measurements are upper limits rather than detections. We argue that this measurement is probably an upper limit, too. This point

is strengthened by the fact that the period measurements from the catalogue of Irwin et al. (2011, solid points in Fig. 10) seem to be rather robust – all periods except for GJ 1186 are consistent with $v \sin i$ data.

7. SUMMARY

We presented a comprehensive catalogue of projected rotation velocities in presumably single stars of spectral type M0.0–M4.5 from high-resolution spectroscopy using 206 new spectra taken for this project and literature values from field stars from several earlier collections. Where available, we add information on chromospheric emission from H α . Our catalogue presents statistically meaningful information on rotation and activity in stars close to the transition between partial and complete convection.

In addition, we identified 12 spectroscopic binaries plus 8 binaries that were already known from earlier work and re-observed for our project. 13 other stars were found to show peculiar line profiles perhaps due to binarity. These 33 stars are not contained in the catalogue and presented individually.

We investigated rotation and activity in our sample stars with an emphasis on the transition from partial to convection convection occurring around spectral type M3. We confirm that the fraction of active stars is very low in early-M stars (<M3) and rises steeply around spectral type M3. For the seven active early-M field stars in our sample, we found evidence that all are younger than a few hundred Myr. Furthermore, find that the behavior of the fraction of rapidly rotating stars with respect to spectral class is virtually identical to the fraction of active stars, which provides strong support to the assumption that all active stars are rapid rotators. Detailed analysis of the rotation-activity relation supports this picture. We argue that in a few individual cases reports of rotational broadening in the absence of H α emission are spurious and that these detections are in fact upper limits of $v \sin i$. We conclude that all rapid rotators ($v \sin i > 3 \text{ km s}^{-1}$) are active ($\log L_{\text{H}\alpha}/L_{\text{bol}} > -4.5$). There is no significant difference between rotation-activity relations on both sides of the convection boundary. An important result is that the distribution of activity in early- to mid-M dwarfs can entirely be explained by rotational braking. This implies that at the boundary to complete convection, we do not observe any evidence for a transition from a rotationally dominated dynamo to a turbulent dynamo independent of rotation. This does not imply that the predominant dynamo mechanism does not change, but it shows that the dynamo in fully convective stars at spectral type M3.0–M4.5 is still driven by rotation.

Scatter in the rotation-activity diagram appears to be different between early-M and later stars (M3.0–M4.5). Early-M stars show less scatter in activity while large scatter is observed in the later ones. The difference, however, is statistically not well defined because the early-M sample consists of five detections in $v \sin i$ only, and the distribution of the slowest rotators among the most active stars among the later-M sample is consistent with random distribution of rotation axes. Some stars also may have been observed during short-time flares.

We compared projected rotation velocities to photometric periods taken from several catalogues. Inclination angles of a few rapid rotators are reported: most

of the stars with rotation periods longer than $P = 10 \text{ d}$ have rotation velocities $v \sin i$ below our detection limit and are consistent with very slow rotation. We identified a few cases where $v \sin i$ and P are inconsistent, in four or five cases the rotation periods are probably mis-identifications, in one case the $v \sin i$ measurement probably is an upper limit rather than a detection.

Our catalogue presents a comprehensive database for understanding the evolution of low-mass stars and the connection between rotation and magnetic activity. The latter is considered as an important factor for the development of life on habitable planets, for which early-M dwarfs have become a prominent target sample. The potential to detect extrasolar planets depends on the width of the stellar line profiles, and our catalogue provides important input selecting target samples for future radial velocity surveys for planets around low-mass stars.

Based on observations collected at the Centro Astronómico Hispano Alemán (CAHA) at Calar Alto, operated jointly by the Max-Planck Institut für Astronomie and the Instituto de Astrofísica de Andalucía (CSIC), and on observations obtained from the European Southern Observatory on MPI time under PID 076.A-9005. AR acknowledges financial support from the Deutsche Forschungsgemeinschaft (DFG) under an Emmy Noether fellowship (RE 1664/4-1) and a Heisenberg Professorship (RE 1664/9-1). NJ acknowledges the support from the DFG Research Training Group GrK-1351 “Extrasolar Planets and their Host Stars”. This work was supported by Sonderforschungsbereich SFB 881 “The Milky Way System” (subproject B6) of the DFG. We thank an anonymous referee for a timely and very useful report.

Facilities: La Silla(FEROS), Calar Alto(FOCES)

REFERENCES

- Alekseev, I. Y. 1998, *Astronomy Reports*, 42, 649
- Baraffe, I., Chabrier, G., Allard, F., & Hauschildt, P. H. 1998, *A&A*, 337, 403
- Basri, G., Mohanty, S., Allard, F., et al. 2000, *ApJ*, 538, 363
- Benedict, G. F., McArthur, B., Nelan, E., et al. 1998, *AJ*, 116, 429
- Beuzit, J.-L., Ségransan, D., Forveille, T., et al. 2004, *Astronomy and Astrophysics*, 425, 997
- Bochanski, J. J., Hawley, S. L., Covey, K. R., et al. 2010, *AJ*, 139, 2679
- Browning, M. K. 2008, *The Astrophysical Journal*, 676, 1262
- Browning, M. K., Basri, G., Marcy, G. W., West, A. A., & Zhang, J. 2010, *The Astronomical Journal*, 139, 504
- Burgasser, A. J., Simcoe, R. A., Bochanski, J. J., et al. 2010, *ApJ*, 725, 1405
- Burningham, B., Leggett, S. K., Homeier, D., et al. 2011, *MNRAS*, 414, 3590
- Cayrel, R. 1988, *The Impact of Very High S/N Spectroscopy on Stellar Physics: Proceedings of the 132nd Symposium of the International Astronomical Union held in Paris*, 132, 345
- Chabrier, G., & Baraffe, I. 1997, *Astronomy and Astrophysics*, 327, 1039
- Contadakis, M. E. 1995, *A&A*, 300, 819
- Cram, L. E., & Mullan, D. J. 1979, *Astrophysical Journal*, 234, 579
- da Silva, L., Torres, C. A. O., de La Reza, R., et al. 2009, *Astronomy and Astrophysics*, 508, 833
- Daemgen, S., Siegler, N., Reid, I. N., & Close, L. M. 2007, *The Astrophysical Journal*, 654, 558
- Delfosse, X., Forveille, T., Perrier, C., & Mayor, M. 1998, *Astronomy and Astrophysics*, 331, 581
- Delfosse, X., Forveille, T., Ségransan, D., et al. 2000, *A&A*, 364, 217

- Demory, B.-O., Ségransan, D., Forveille, T., et al. 2009, *A&A*, 505, 205
- Donati, J.-F., Morin, J., Petit, P., et al. 2008, *Monthly Notices of the Royal Astronomical Society*, 390, 545
- Engle, S. G., Guinan, E. F., & Mizusawa, T. 2009, in *American Institute of Physics Conference Series*, Vol. 1135, American Institute of Physics Conference Series, ed. M. E. van Steenberg, G. Sonneborn, H. W. Moos, & W. P. Blair, 221–224
- Fekel, F. C., & Henry, G. W. 2000, *AJ*, 120, 3265
- Femenía, B., Rebolo, R., Pérez-Prieto, J. A., et al. 2011, *MNRAS*, 413, 1524
- Gizis, J. E., Reid, I. N., & Hawley, S. L. 2002, *AJ*, 123, 3356
- Goldman, B., Marsat, S., Henning, T., Clemens, C., & Greiner, J. 2010, *Monthly Notices of the Royal Astronomical Society*, 405, 1140
- Gray, D. F. 2005, *The Observation and Analysis of Stellar Photospheres* (Cambridge University Press)
- Hauschildt, P. H., Allard, F., & Baron, E. 1999, *The Astrophysical Journal*, 512, 377
- Hawley, S. L., Gizis, J. E., & Reid, I. N. 1996, *Astronomical Journal* v.112, 112, 2799
- Hilton, E. J., West, A. A., Hawley, S. L., & Kowalski, A. F. 2010, *AJ*, 140, 1402
- Irwin, J., Berta, Z. K., Burke, C. J., et al. 2011, *ApJ*, 727, 56
- Jenkins, J. S., Ramsey, L. W., Jones, H. R. A., et al. 2009, *The Astrophysical Journal*, 704, 975
- Kenyon, S. J., & Hartmann, L. 1995, *Astrophysical Journal Supplement* v.101, 101, 117
- Kiraga, M., & Stepien, K. 2007, *Acta Astron.*, 57, 149
- Kowalski, A. F., Hawley, S. L., Hilton, E. J., et al. 2009, *AJ*, 138, 633
- Lee, K.-G., Berger, E., & Knapp, G. R. 2010, *ApJ*, 708, 1482
- Marcy, G. W., & Chen, G. H. 1992, *Astrophysical Journal*, 390, 550
- Messina, S., Pizzolato, N., Guinan, E. F., & Rodonò, M. 2003, *A&A*, 410, 671
- Mohanty, S., & Basri, G. 2003, *The Astrophysical Journal*, 583, 451
- Morin, J., Donati, J.-F., Petit, P., et al. 2008, *Monthly Notices of the Royal Astronomical Society*, 390, 567
- Noyes, R. W., Hartmann, L. W., Baliunas, S. L., Duncan, D. K., & Vaughan, A. H. 1984, *Astrophysical Journal*, 279, 763
- Ossendrijver, M. 2003, *The Astronomy and Astrophysics Review*, 11, 287
- Parker, E. N. 1993, *Astrophysical Journal*, 408, 707
- Pizzolato, N., Maggio, A., Micela, G., Sciortino, S., & Ventura, P. 2003, *Astronomy and Astrophysics*, 397, 147
- Press, W. H., Teukolsky, S. A., Vetterling, W. T., & Flannery, B. P. 1992, *Numerical recipes in C. The art of scientific computing*, ed. Press, W. H., Teukolsky, S. A., Vetterling, W. T., & Flannery, B. P.
- Reid, I. N., Hawley, S. L., & Gizis, J. E. 1995, *Astronomical Journal* v.110, 110, 1838
- Reiners, A. 2007, *Astronomy and Astrophysics*, 467, 259
- Reiners, A., & Basri, G. 2007, *The Astrophysical Journal*, 656, 1121
- Reiners, A., & Basri, G. 2008, *A&A*, 489, L45
- . 2010, *ApJ*, 710, 924
- Reiners, A., & Mohanty, S. 2011, *ArXiv e-prints*
- Shkolnik, E., Liu, M. C., & Reid, I. N. 2009, *The Astrophysical Journal*, 699, 649
- Shulyak, D., Seifahrt, A., Reiners, A., Kochukhov, O., & Piskunov, N. 2011, *MNRAS*, 1579
- Silvestri, N. M., Hawley, S. L., & Oswalt, T. D. 2005, *AJ*, 129, 2428
- Simon, M., Bender, C., & Prato, L. 2006, *ApJ*, 644, 1183
- Tonry, J., & Davis, M. 1979, *Astronomical Journal*, 84, 1511
- Torres, C. A. O., Quast, G. R., da Silva, L., et al. 2006, *A&A*, 460, 695
- West, A. A., & Basri, G. 2009, *ApJ*, 693, 1283
- West, A. A., Hawley, S. L., Bochanski, J. J., et al. 2008, *AJ*, 135, 785
- West, A. A., Hawley, S. L., Walkowicz, L. M., et al. 2004, *The Astronomical Journal*, 128, 426
- Zuckerman, B., Bessell, M. S., Song, I., & Kim, S. 2006, *ApJ*, 649, L115

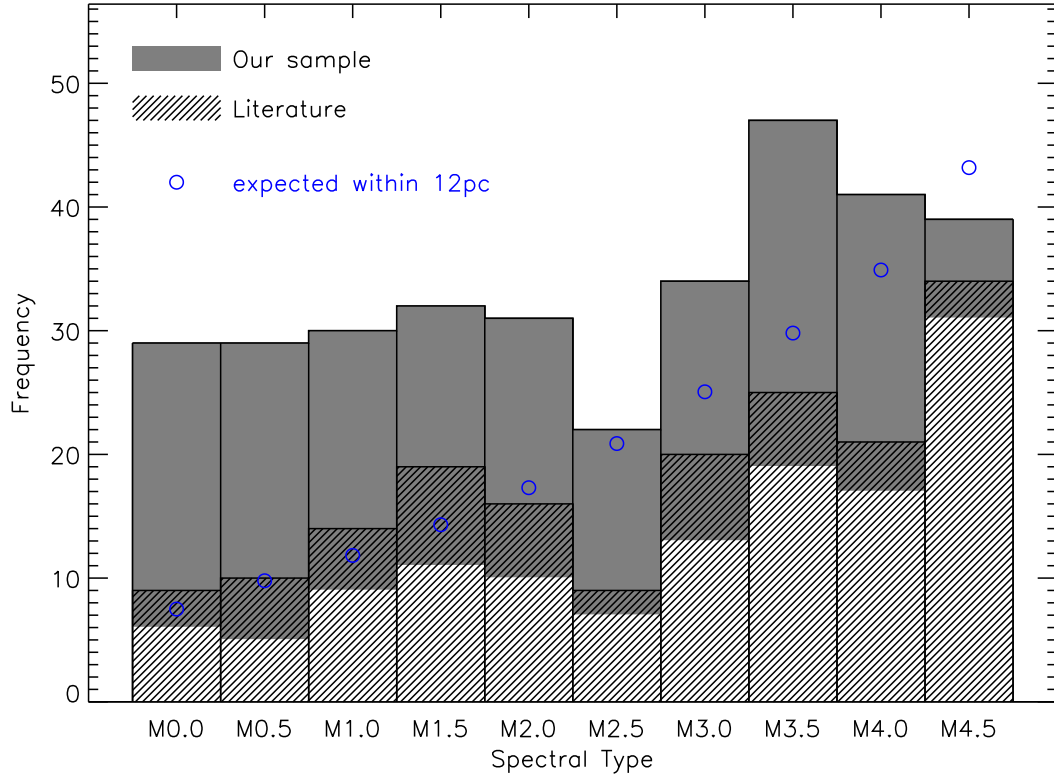


Figure 1. Spectral type distribution of our catalogue. The fraction of stars observed within the course of this project is shown in grey, stars taken from the literature are shown as hatched histogram. Blue circles show expected numbers of stars per spectral bin contained within 12 pc according to the mass function from Bochanski et al. (2010).

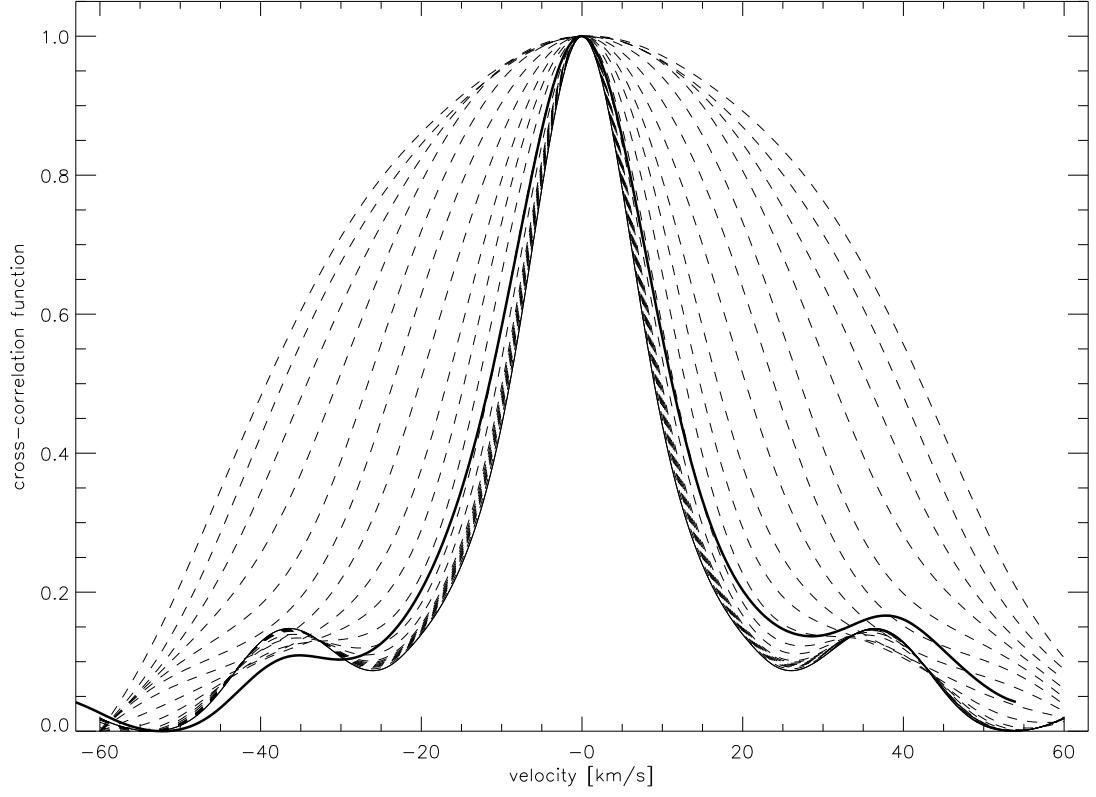


Figure 2. Typical cross-correlation profiles. Dashed lines show cross-correlation functions of artificially broadened spectra with the template spectrum. The dark line is the cross-correlation function from an object spectrum with the template spectrum.

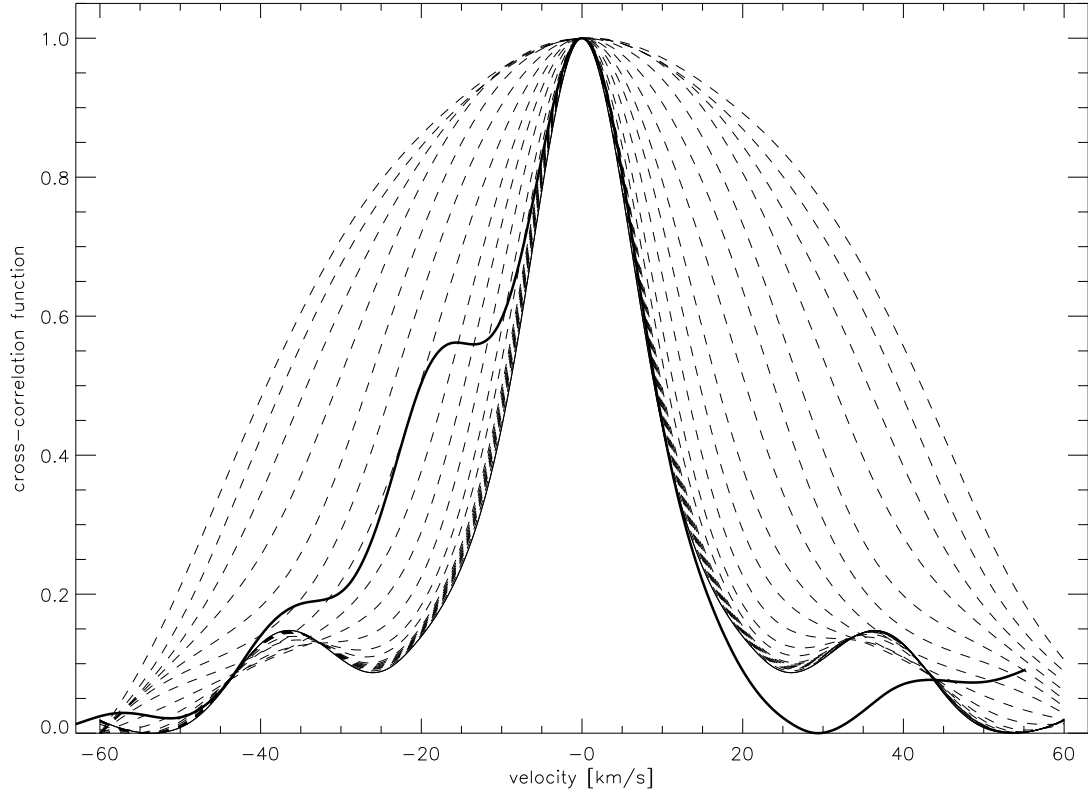


Figure 3. Cross-correlation profile of a probable spectroscopic binary. Dashed lines show cross-correlations function of artificially broadened spectra with the template spectrum. The dark line is the cross-correlation function from an object spectrum with the template spectrum.

Table 5
Stars with photometric periods

Name	Spectral type	P [d]	ref	v_{eq} [km s ⁻¹]	$v \sin i$ [km s ⁻¹]	ref	i [°]	exceed
G1 182	M0.0	4.4	(ks)	7.9	10.4	(1)		1.3
G1 410	M0.0	14.8	(fh)	2.0	< 2.5	(2)		
G1 424	M0.0	149.7	(en)	0.2	< 2.5	(2)		
G1 494	M0.5	2.9	(ks)	9.8	9.7	(2)	81	
Steph 546A	M1.5	0.3	(ks)	74.2	5.3	(1)	4	
G1 205	M1.5	33.6	(ks)	0.9	1.5	(4)		1.7
G1 382	M1.5	21.6	(ks)	1.2	1.8	(4)		1.5
Wo 9520	M1.5	0.4	(ks)	69.9	6.5	(1)	5	
GJ 2036A	M2.0	0.8	(ks)	22.6	44.3	(1)		2.0
G1 358	M2.0	25.3	(ks)	0.8	< 3.0	(1)		
G1 411	M2.0	48.0	(no)	0.5	< 2.5	(2)		
G1 569A	M2.0	13.7	(ks)	1.7	< 2.5	(2)		
G1 84	M2.5	44.5	(ks)	0.5	< 3.0	(1)		
G1 674	M2.5	33.3	(ks)	0.6	< 3.0	(1)		
G1 388	M3.0	2.2	(en)	8.2	3.0	(4)	21	
G1 735	M3.0	2.9	(al)	9.0	7.7	(1)	58	
G1 431	M3.5	14.3	(ks)	1.2	20.5	(1)		17.6
G1 669A	M3.5	0.9	(ks)	18.6	< 4.0	(1)	12	
G1 729	M3.5	2.9	(ks)	3.5	4.0	(2)		1.1
G1 873	M3.5	4.4	(co)	3.4	3.5	(2)		1.0
G 099-049	M4.0	1.8	(ir)	7.3	7.4	(5)		1.0
G1 699	M4.0	130.0	(be)	0.1	< 2.5	(2)		
GJ 1243	M4.0	0.6	(ir)	22.2	22.0	(1)	83	
G1 876	M4.0	116.5	(en)	0.1	< 2.5	(2)		
LHS 1885	M4.5	52.4	(ir)	0.2	< 3.7	(5)		
G1 285	M4.5	2.8	(ir)	5.8	4.5	(4)	50	
GJ 1151	M4.5	132.0	(ir)	0.1	< 4.1	(5)		
G1 493.1	M4.5	0.6	(ir)	16.0	16.8	(5)		1.0
GJ 1186	M4.5	88.3	(ir)	0.1	3.9	(6)		40.1
G1 791.2	M4.5	0.3	(ir)	33.6	32.0	(5)	72	
GJ 1057	M5.0	102.0	(ir)	0.1	< 2.2	(5)		
GJ 1156	M5.0	0.5	(ir)	16.5	9.2	(5)	33	
G1 551	M5.5	82.5	(ks)	0.1	< 3.0	(8)		

References. — Period references: (ks) Kiraga & Stepien (2007); (fh) Fekel & Henry (2000); (no) Noyes et al. (1984); (al) Alekseev (1998); (be) Benedict et al. (1998); (ir) Irwin et al. (2011); (en) Engle et al. (2009); (co) Contadakis (1995) – $v \sin i$ references: (1) This work (2) Browning et al. (2010); (3) Marcy & Chen (1992); (4) Reiners (2007); (5) Delfosse et al. (1998); (6) Jenkins et al. (2009); (7) Reiners & Basri (2007); (8) Reiners & Basri (2008)

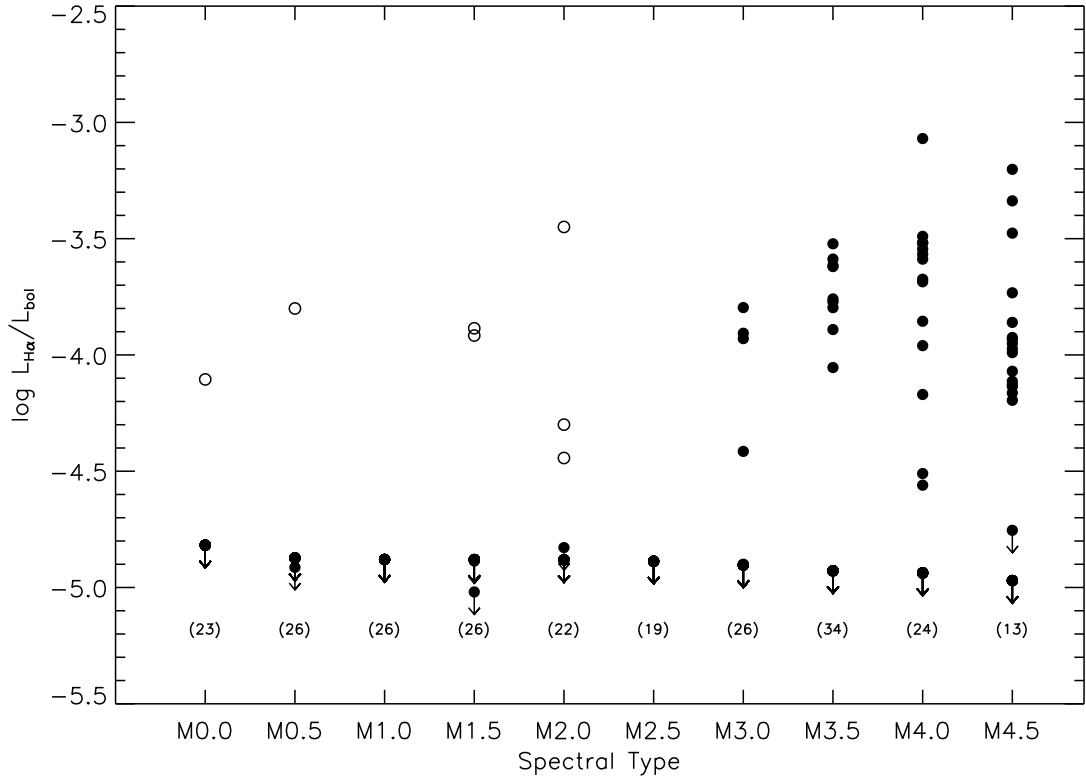


Figure 4. Normalized H α luminosities as a function of spectral type. Early-M dwarfs (<M3) with significant H α detections are shown as open circles, all other targets as full circles. Non-detections of H α are plotted at their detection levels with downward arrows added at their position. Numbers in parentheses show the number of non-detections per spectral bin that are often overplotted at the same position.

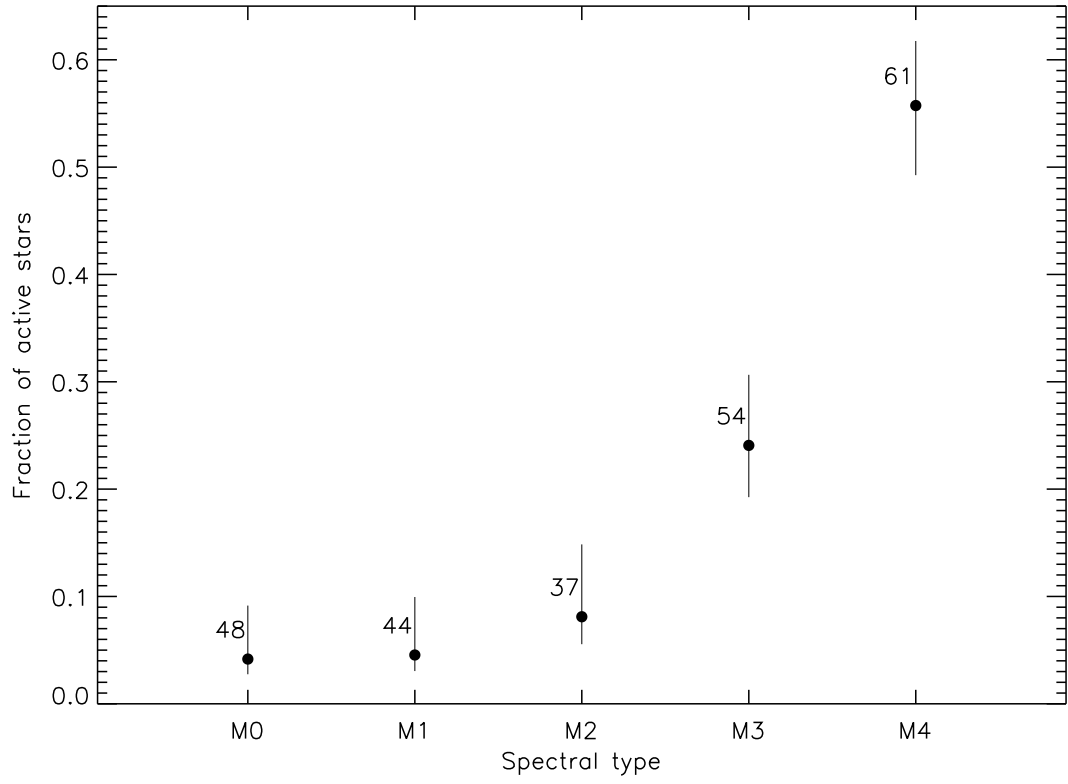


Figure 5. Fraction of active stars per spectral type in our sample. Numbers show how many stars are measured per spectral bin. Error bars show 1σ -uncertainties.

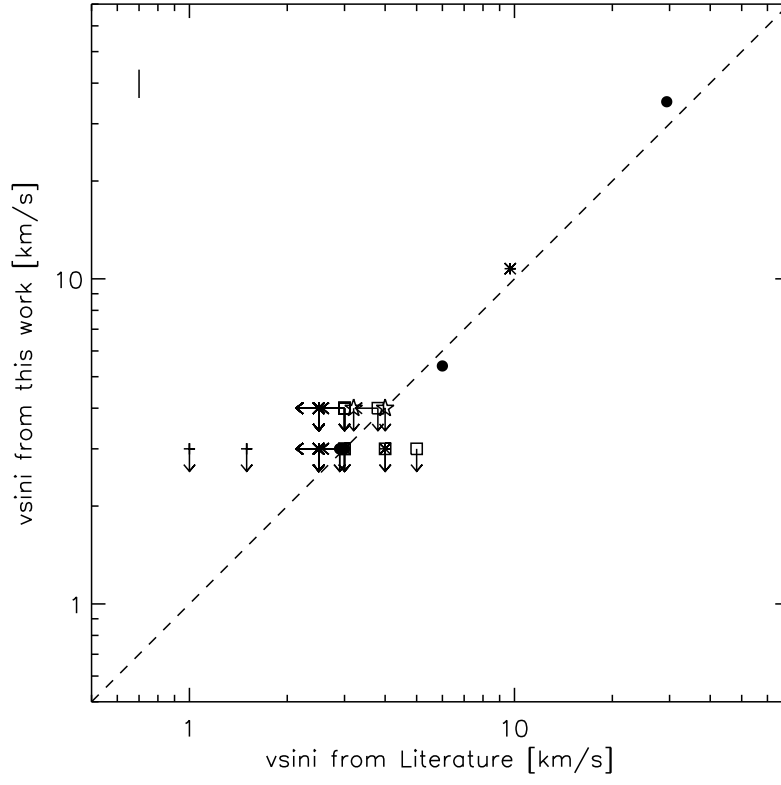


Figure 6. Comparison between $v \sin i$ values from this work and the literature. Different symbols are used for different literature sources (see Table 7).

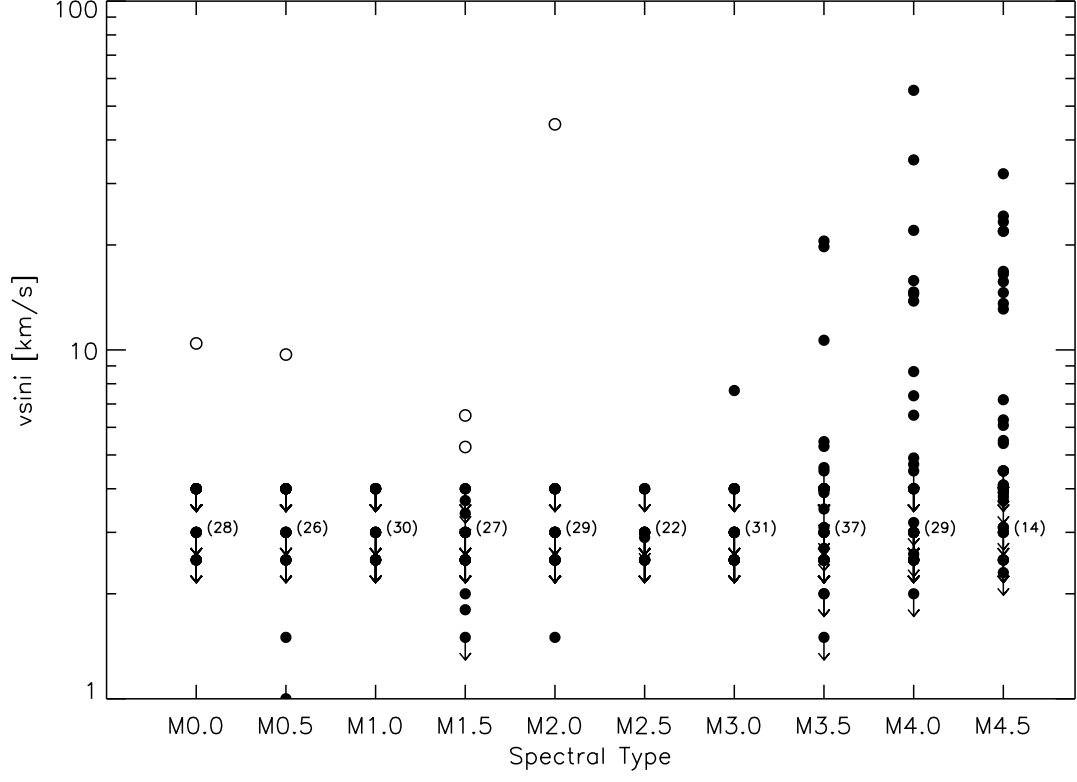


Figure 7. Projected rotational velocity ($v \sin i$) as a function of spectral type. Upper limits in $v \sin i$ are shown with downward arrows. Open circles show early-type M stars ($< M3$) that were found to be rotating faster than $v \sin i = 3 \text{ km s}^{-1}$ (five stars). The numbers in parentheses denote the numbers of slow rotators per spectral bin in which rotation is below the detection threshold (sum of all stars with downward arrows in this bin).

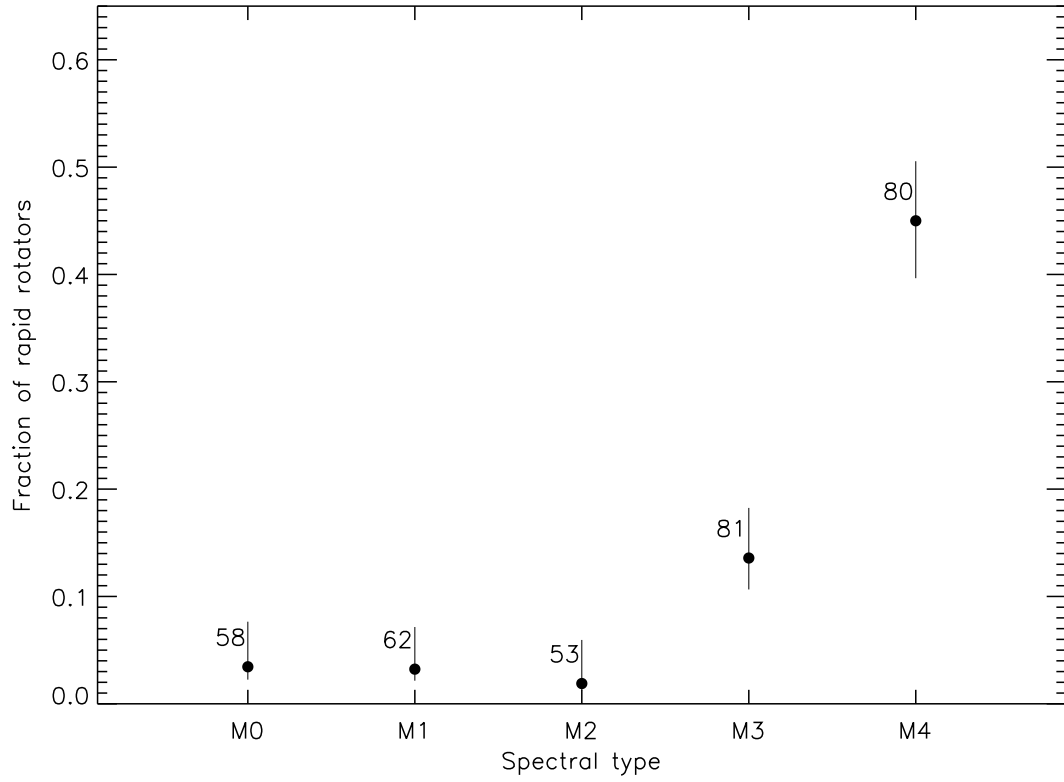


Figure 8. Fraction of rapid rotators per spectral type in our sample. Rapid rotators are stars with detected rotational broadening at $v \sin i = 3 \text{ km s}^{-1}$ or larger. Numbers show how many stars are measured per spectral bin. Error bars show 1σ -uncertainties.

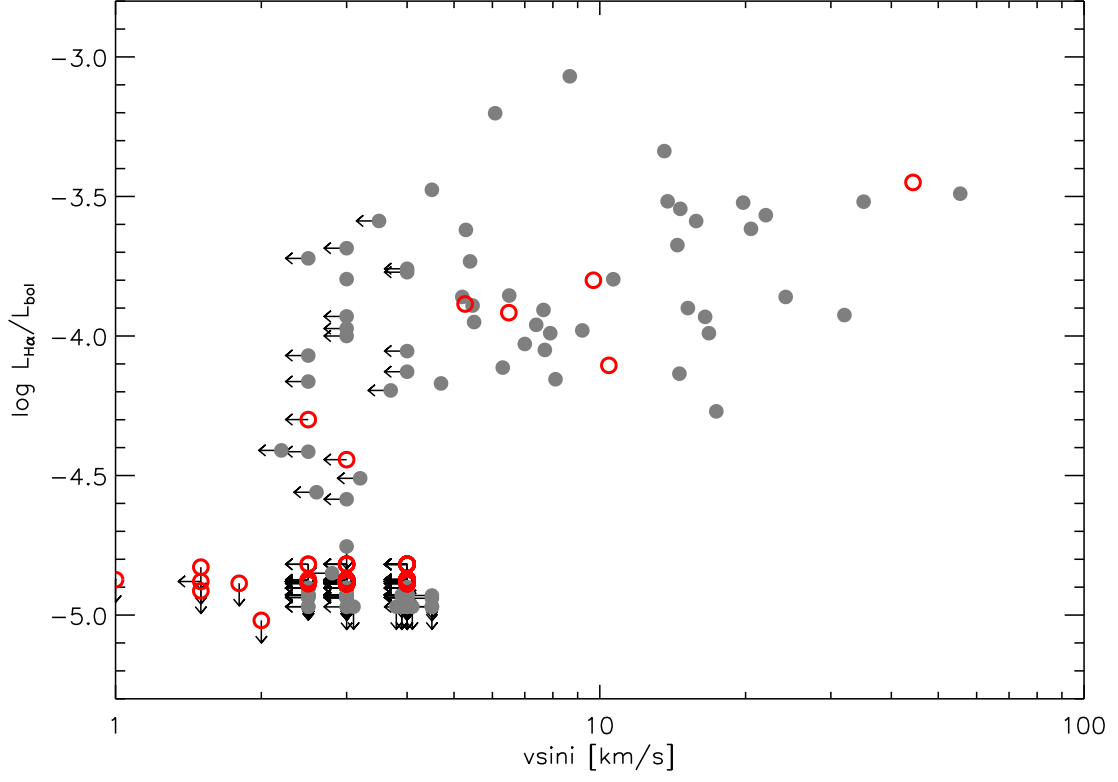


Figure 9. Normalized $H\alpha$ luminosity as a function of projected rotational velocity ($v \sin i$). Open circles denote partially convective objects (M0.0–M2.5), whereas filled circles show fully convective ones (M3.0–M4.5). Leftward arrows show objects with upper limits in $v \sin i$, downward arrows show upper limits in $H\alpha$ activity.

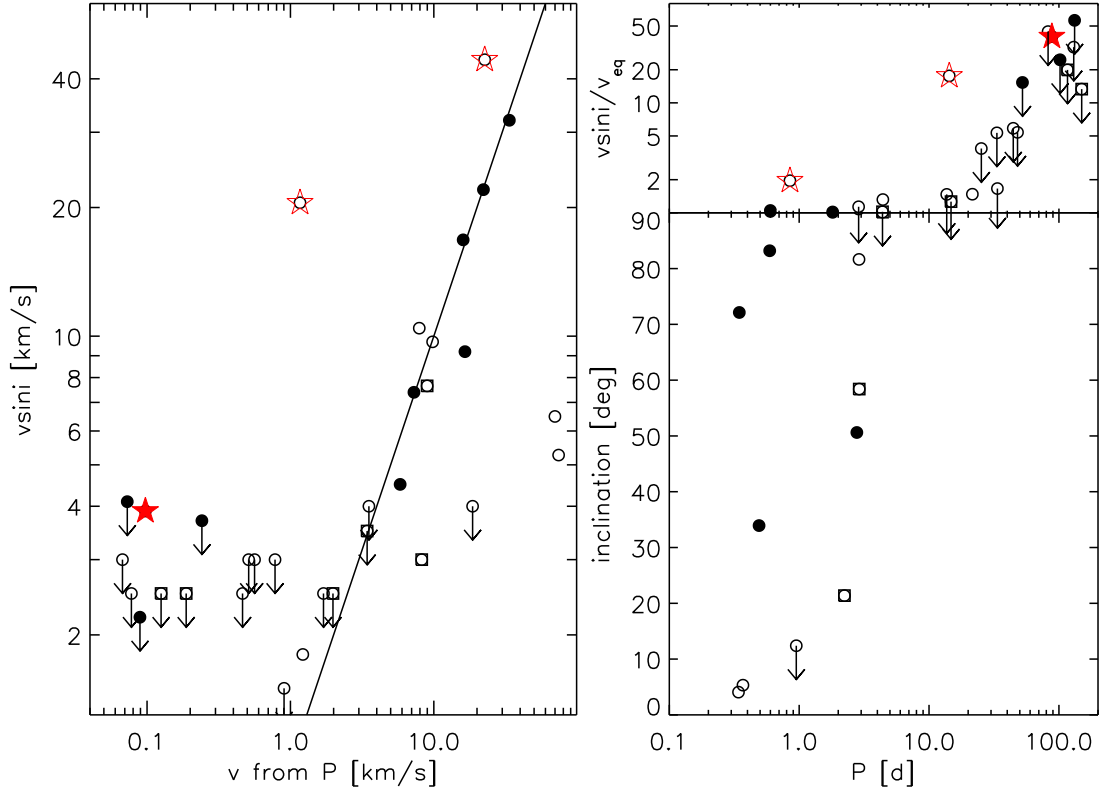


Figure 10. *Left panel:* Projected rotational velocity $v \sin i$ against surface equatorial velocity v_{eq} calculated from photometric period. *Right panel:* Inclination angle derived from the comparison between $v \sin i$ and v_{eq} if $v \sin i < v_{\text{eq}}$ (lower panel), and ratio $v \sin i / v_{\text{eq}}$ if $v \sin i > v_{\text{eq}}$ (upper panel). Downward arrows indicate upper limits in all values that are due to upper limits in $v \sin i$. Solid symbols are period measurements from Irwin et al. (2011), open circles are from Kiraga & Stepień (2007), open squares are taken from other literature (see text). Three stars with $v \sin i > v_{\text{eq}}$ in which $v \sin i$ is not an upper limit are shown as red stars.

Table 6
Catalogue of rotation and activity in 334 M0–M4.5 stars

Name	$\alpha(J2000)$	$\delta(J2000)$	Spectral type	$\log(L_{H_\alpha}/L_{bol})$	$v \sin i$ [km s ⁻¹]	ref
LTT 692	01 14 33.9	−53 56 39	M0.0	< −4.82	< 3.0	(1)
LTT 11085	03 18 38.1	32 39 57	M0.0	< −4.82	< 4.0	(1)
Gl 182	04 59 34.7	01 47 00	M0.0	−4.11	10.4	(1)
Gl 353	09 31 56.4	36 19 16	M0.0	–	< 2.5	(2)
Gl 373	09 56 08.9	62 47 21	M0.0	–	< 2.5	(2)
Gl 410	11 02 38.2	21 58 01	M0.0	–	< 2.5	(2)
Gl 424	11 19 57.7	65 50 33	M0.0	–	< 2.5	(2)
Gl 438	11 43 18.1	−51 50 14	M0.0	< −4.82	< 3.0	(1)
Gl 459.3	12 19 24.4	28 22 55	M0.0	–	< 3.0	(3)
Gl 461A	12 20 25.4	00 34 59	M0.0	–	< 3.0	(3)
Gl 548A	14 25 42.9	23 37 10	M0.0	< −4.82	< 4.0	(1)
V 759	16 09 02.9	52 56 36	M0.0	< −4.82	< 4.0	(1)
V 791	17 18 21.6	−01 46 51	M0.0	< −4.82	< 4.0	(1)
Gl 676A	17 30 11.6	−51 38 11	M0.0	< −4.82	< 3.0	(1)
Gl 678.1A	17 30 22.6	05 32 55	M0.0	< −4.82	< 2.5	(2)
Gl 694.2	17 45 33.4	46 51 18	M0.0	< −4.82	< 4.0	(1)
Gl 696	17 50 33.9	−06 02 59	M0.0	< −4.82	< 4.0	(1)
G 183-041	18 25 04.7	24 38 08	M0.0	< −4.82	< 4.0	(1)
Gl 720A	18 35 18.0	45 44 35	M0.0	< −4.82	< 3.0	(3)
Gl 731	18 51 51.2	16 35 03	M0.0	< −4.82	< 4.0	(1)
G 141-052	18 59 38.3	07 59 14	M0.0	< −4.82	< 4.0	(1)
V 811A	19 35 06.3	08 27 39	M0.0	< −4.82	< 4.0	(1)
G 260-030	19 39 33.1	71 52 22	M0.0	< −4.82	< 4.0	(1)
G 210-045	20 58 41.7	34 16 27	M0.0	< −4.82	< 4.0	(1)
Gl 835	21 38 00.0	27 43 25	M0.0	< −4.82	< 4.0	(1)
Gl 838.3B	21 51 53.3	42 20 39	M0.0	< −4.82	< 4.0	(1)
Gl 839	21 53 58.7	41 46 46	M0.0	< −4.82	< 4.0	(1)
Gl 846	22 02 10.4	01 24 02	M0.0	< −4.82	< 2.5	(2)
Wo 9784	22 28 45.8	18 55 54	M0.0	< −4.82	< 4.0	(1)
LHS 1051A	00 15 49.3	−67 59 49	M0.5	< −4.87	< 3.0	(1)
GJ 2003	00 20 08.2	−17 03 38	M0.5	< −4.87	< 3.0	(1)
Gl 21	00 26 52.9	70 08 33	M0.5	< −4.87	< 4.0	(1)
Gl 27.1	00 39 57.8	−44 15 08	M0.5	< −4.87	< 3.0	(2)
Gl 84.1A	02 05 23.3	−28 04 16	M0.5	< −4.87	< 3.0	(1)
Gl 155.1	03 47 58.2	02 47 18	M0.5	< −4.87	< 3.0	(1)
GJ 1074	04 58 45.5	50 56 39	M0.5	< −4.87	< 4.0	(1)
Gl 184	05 03 22.7	53 07 55	M0.5	< −4.87	< 4.0	(1)
Gl 212	05 41 30.7	53 29 27	M0.5	< −4.87	< 2.5	(2)
Gl 229	06 10 34.6	−21 51 46	M0.5	< −4.87	1.0	(4)
Gl 277.1	07 34 28.1	62 56 30	M0.5	–	< 2.5	(2)
Gl 336.1	09 11 31.0	46 37 01	M0.5	< −4.87	< 4.0	(1)
Gl 369	09 51 08.9	−12 19 34	M0.5	< −4.87	< 3.0	(1)
Gl 412A	11 05 24.6	43 31 41	M0.5	–	< 2.5	(2)
Gl 494	13 00 46.8	12 22 32	M0.5	−3.80	9.7	(2)
Gl 507A	13 19 33.3	35 06 41	M0.5	< −4.87	< 4.0	(1)
Gl 514	13 29 59.0	10 22 46	M0.5	< −4.91	1.5	(4)
V 150	14 02 19.5	13 41 24	M0.5	< −4.87	< 4.0	(1)
Gl 537A	14 02 32.7	46 20 24	M0.5	< −4.87	< 4.0	(1)
Gl 537B	14 02 32.7	46 20 24	M0.5	< −4.87	< 4.0	(1)
Gl 548B	14 25 46.1	23 37 22	M0.5	< −4.87	< 4.0	(1)
Steph 1453	17 15 50.2	18 59 58	M0.5	< −4.87	< 4.0	(1)
Gl 685	17 35 34.0	61 40 57	M0.5	< −4.87	< 4.0	(1)
G 182-037	18 04 17.5	35 57 27	M0.5	< −4.87	< 4.0	(1)
Gl 709	18 16 31.0	45 33 24	M0.5	< −4.87	< 4.0	(1)
Gl 740	18 58 00.1	05 54 36	M0.5	< −4.87	< 4.0	(1)
Gl 809	20 53 19.7	62 09 20	M0.5	–	< 2.5	(2)
Gl 842.2	21 58 24.2	75 35 19	M0.5	< −4.87	< 4.0	(1)
Gl 887	23 05 52.0	−35 51 12	M0.5	–	< 2.5	(2)
Gl 2	00 05 10.2	45 47 12	M1.0	< −4.88	< 2.5	(2)
Gl 15A	00 18 20.8	44 01 19	M1.0	–	< 2.5	(2)
G 036-038	02 52 24.9	26 58 31	M1.0	< −4.88	< 4.0	(1)
Gl 119A	02 56 33.7	55 26 15	M1.0	< −4.88	< 4.0	(1)
G 246-026	03 10 26.4	58 26 08	M1.0	< −4.88	< 4.0	(1)
Gl 140A	03 24 06.4	23 47 06	M1.0	< −4.88	< 4.0	(1)
Gl 150.1B	03 43 45.1	16 40 03	M1.0	< −4.88	< 3.0	(1)
Wo 9163A	04 40 29.2	−09 11 44	M1.0	< −4.88	< 3.0	(1)
G 081-036	04 50 15.1	45 58 51	M1.0	< −4.88	< 4.0	(1)
Gl 367	09 44 30.5	−45 46 25	M1.0	< −4.88	< 3.0	(1)
Gl 390	10 25 11.0	−10 13 44	M1.0	< −4.88	< 2.5	(2)
Gl 450	11 51 07.5	35 16 16	M1.0	–	< 2.5	(2)
Gl 477	12 35 58.6	−45 56 05	M1.0	< −4.88	< 3.0	(1)
Gl 521	13 39 24.1	46 11 07	M1.0	–	< 3.0	(3)
Gl 536	14 01 03.7	−02 39 23	M1.0	< −4.88	< 2.5	(2)

Table 6 — *Continued*

Name	$\alpha(J2000)$	$\delta(J2000)$	Spectral type	$\log(L_{H\alpha}/L_{bol})$	$v \sin i$ [km s ⁻¹]	ref
Gl 570B	14 57 27.3	-21 25 02	M1.0	—	< 2.5	(2)
Gl 606	15 59 53.1	-08 15 11	M1.0	< -4.88	< 3.0	(1)
LP 806-8	16 48 45.8	-15 44 17	M1.0	< -4.88	< 4.0	(1)
Gl 649	16 58 08.8	25 44 41	M1.0	< -4.88	< 2.5	(2)
G 139-023	17 16 00.6	11 03 29	M1.0	< -4.88	< 4.0	(1)
Gl 686	17 37 52.7	18 35 21	M1.0	—	< 2.5	(2)
Gl 701	18 05 07.0	-03 01 47	M1.0	—	< 2.5	(2)
Gl 724	18 40 57.3	-13 22 42	M1.0	< -4.88	< 4.0	(1)
G 125-030	19 45 49.4	32 23 10	M1.0	< -4.88	< 4.0	(1)
Gl 767A	19 46 23.7	32 01 02	M1.0	< -4.88	< 4.0	(1)
G 262-029	20 51 59.7	69 10 07	M1.0	< -4.88	< 4.0	(1)
Gl 821	21 09 17.0	-13 17 54	M1.0	< -4.88	< 2.5	(2)
Gl 863	22 33 01.9	09 22 40	M1.0	—	< 3.0	(3)
Gl 895	23 24 30.4	57 51 17	M1.0	—	< 2.5	(2)
Gl 908	23 49 11.9	02 24 11	M1.0	—	< 2.5	(2)
Gl 1	00 05 24.4	-37 21 25	M1.5	< -4.88	< 2.5	(2)
G 242-048A	00 13 39.9	80 39 26	M1.5	< -4.88	< 4.0	(1)
Gl 16	00 18 16.5	10 12 09	M1.5	< -4.88	< 3.0	(1)
GJ 1009	00 21 55.8	-31 24 18	M1.5	< -4.88	< 2.5	(2)
Gl 49	01 02 38.0	62 20 40	M1.5	—	< 3.4	(5)
Gl 87	02 12 21.8	03 34 45	M1.5	< -4.88	< 2.5	(2)
Gl 91	02 13 52.3	-32 02 19	M1.5	< -4.88	< 3.0	(1)
GJ 1051	02 43 52.6	-08 49 36	M1.5	< -4.88	< 3.0	(1)
Gl 114.1A	02 50 03.6	-53 08 36	M1.5	< -4.88	< 3.0	(1)
Gl 156.1A	03 56 47.1	53 33 39	M1.5	< -4.88	< 4.0	(1)
Gl 173	04 37 41.9	-11 02 18	M1.5	< -4.88	< 2.5	(2)
Steph 546A	05 06 49.6	-21 35 06	M1.5	-3.89	5.3	(1)
Gl 205	05 31 26.9	-03 40 22	M1.5	< -4.88	1.5	(4)
Gl 218	05 47 39.3	-36 19 41	M1.5	< -4.88	< 3.0	(1)
LTT 3412	09 16 20.9	-18 37 35	M1.5	< -4.88	< 3.0	(1)
Gl 361	09 41 10.6	13 12 34	M1.5	—	< 2.5	(2)
Gl 382	10 12 17.6	-03 44 42	M1.5	< -4.89	1.8	(4)
Gl 414B	11 11 02.2	30 26 42	M1.5	—	< 2.5	(2)
Steph 928	11 12 38.9	18 56 04	M1.5	< -4.88	< 3.0	(1)
Gl 433	11 35 27.1	-32 32 08	M1.5	—	< 2.5	(2)
GJ 2097	13 07 04.3	20 48 38	M1.5	—	< 3.7	(5)
Gl 507.1	13 19 40.2	33 20 47	M1.5	—	< 3.0	(3)
Gl 526	13 45 42.8	14 53 39	M1.5	< -5.02	2.0	(4)
Wo 9492	14 42 21.8	66 03 19	M1.5	< -4.88	< 2.5	(2)
Wo 9520	15 21 52.8	20 58 38	M1.5	-3.92	6.5	(1)
Gl 625	16 25 24.1	54 18 15	M1.5	—	< 2.5	(2)
Gl 667C	17 18 57.7	-34 59 46	M1.5	< -4.88	< 2.5	(2)
Gl 680	17 35 13.6	-48 40 55	M1.5	< -4.88	< 3.0	(1)
Gl 745A	19 07 05.8	20 53 18	M1.5	—	< 2.5	(2)
Gl 800A	20 42 56.5	-18 54 54	M1.5	< -4.88	< 4.0	(1)
Gl 806	20 45 03.6	44 29 44	M1.5	< -4.88	< 2.5	(2)
Gl 880	22 56 35.3	16 33 13	M1.5	—	< 2.5	(2)
Gl 22A.01	00 32 27.3	67 14 09	M2.0	< -4.88	< 4.0	(1)
Gl 47	01 01 19.6	61 22 02	M2.0	< -4.88	< 4.0	(1)
GJ 1026A	01 03 13.7	20 05 51	M2.0	< -4.88	< 3.0	(1)
GJ 1030	01 06 41.5	15 16 22	M2.0	< -4.88	< 4.0	(1)
Gl 70	01 43 20.3	04 19 23	M2.0	< -4.88	< 2.5	(2)
Gl 78	01 51 48.3	-10 48 08	M2.0	< -4.88	< 3.0	(1)
Gl 133	03 21 20.5	79 57 59	M2.0	< -4.88	< 4.0	(1)
GJ 2036A	04 53 30.8	-55 51 34	M2.0	-3.45	44.3	(1)
Gl 180	04 53 49.6	-17 46 16	M2.0	< -4.88	< 2.5	(2)
Gl 192	05 12 42.0	19 39 53	M2.0	—	< 2.5	(2)
GJ 1077	05 16 59.4	-78 16 54	M2.0	< -4.88	< 3.0	(1)
Gl 226	06 10 19.3	82 06 33	M2.0	< -4.88	< 2.5	(2)
Gl 250B	06 52 18.3	-05 11 22	M2.0	—	< 2.5	(2)
GJ 2066	08 16 08.1	01 18 07	M2.0	—	< 2.5	(2)
Gl 358	09 39 47.3	-41 04 11	M2.0	-4.44	< 3.0	(1)
Gl 372	09 53 11.8	-03 41 20	M2.0	< -4.88	< 4.0	(1)
Gl 393	10 28 55.8	00 50 32	M2.0	< -4.83	1.5	(4)
Gl 411	11 03 22.3	35 57 20	M2.0	—	< 2.5	(2)
Gl 413.1	11 09 32.1	-24 35 49	M2.0	< -4.88	< 2.5	(2)
Gl 465	12 24 51.8	-18 14 16	M2.0	< -4.88	< 2.5	(2)
Gl 479	12 37 54.4	-52 00 06	M2.0	< -4.88	< 3.0	(1)
Gl 552	14 29 30.2	15 31 46	M2.0	—	< 2.5	(2)
Gl 569A	14 54 29.0	16 06 05	M2.0	-4.30	< 2.5	(2)
Gl 618A	16 20 04.9	-37 32 08	M2.0	< -4.88	< 3.0	(1)
LTT 14949	16 40 48.9	36 18 57	M2.0	< -4.88	< 4.0	(1)
Gl 654	17 05 14.1	-05 05 28	M2.0	—	< 3.0	(3)
GJ 2128	17 16 41.1	08 03 30	M2.0	< -4.88	< 4.0	(1)

Table 6 — *Continued*

Name	$\alpha(J2000)$	$\delta(J2000)$	Spectral type	$\log(L_{H\alpha}/L_{bol})$	$v \sin i$ [km s ⁻¹]	ref
Gl 739	18 59 07.1	-48 16 15	M2.0	< -4.88	< 3.0	(1)
Gl 745B	19 07 13.5	20 52 37	M2.0	-	< 2.5	(2)
Gl 851	22 11 29.8	18 25 32	M2.0	-	< 2.5	(2)
Gl 891	23 10 15.0	-25 55 52	M2.0	-	< 2.5	(2)
Gl 26	00 38 58.0	30 36 57	M2.5	< -4.89	< 2.5	(2)
Gl 63	01 38 22.0	57 13 55	M2.5	< -4.89	< 4.0	(1)
G 244-037	01 51 50.8	64 26 07	M2.5	< -4.89	< 4.0	(1)
Gl 84	02 05 04.1	-17 36 51	M2.5	< -4.89	< 3.0	(1)
GJ 1046	02 19 07.7	-36 46 52	M2.5	< -4.89	< 3.0	(1)
Gl 145	03 32 56.5	-44 42 10	M2.5	< -4.89	< 3.0	(1)
Gl 238	06 33 51.1	-58 31 58	M2.5	< -4.89	< 3.0	(1)
GJ 1099	07 34 17.6	00 59 12	M2.5	< -4.89	< 3.0	(1)
Gl 357	09 36 01.5	-21 39 31	M2.5	-	< 2.5	(2)
Gl 381	10 12 04.3	-02 41 00	M2.5	< -4.89	< 4.0	(1)
Gl 399	10 39 40.9	-06 55 23	M2.5	< -4.89	< 4.0	(1)
Gl 408	11 00 04.5	22 50 00	M2.5	-	< 2.5	(2)
Gl 436	11 42 10.5	26 42 30	M2.5	< -4.89	< 2.5	(2)
Gl 476	12 35 00.9	09 49 45	M2.5	< -4.89	< 3.0	(1)
Gl 588	15 32 14.2	-41 16 20	M2.5	< -4.89	< 3.0	(1)
Gl 623	16 24 08.4	48 21 12	M2.5	-	< 2.9	(5)
Gl 671	17 19 52.4	41 42 56	M2.5	-	< 2.5	(2)
Gl 674	17 28 39.2	-46 53 33	M2.5	< -4.89	< 3.0	(1)
Gl 694	17 43 55.8	43 22 47	M2.5	-	< 2.5	(2)
GJ 2138	18 38 44.6	-14 29 22	M2.5	< -4.89	< 3.0	(1)
Gl 752A	19 16 54.7	05 09 55	M2.5	-	< 2.5	(2)
Gl 793	20 30 31.4	65 26 55	M2.5	-	< 2.5	(2)
Gl 22B	00 32 27.3	67 14 09	M3.0	< -4.90	< 4.0	(1)
Gl 48	01 02 29.5	71 40 50	M3.0	-	< 2.5	(2)
GJ 3104	01 39 31.2	05 03 18	M3.0	< -4.90*	4.0	(6)
G 244-047.01	02 01 35.6	63 46 11	M3.0	< -4.90	< 2.5	(2)
LHS 1377A	02 16 40.1	-30 59 23	M3.0	-3.93	< 3.0	(1)
Gl 109	02 44 14.9	25 31 25	M3.0	-	< 2.5	(2)
Gl 119B	02 56 34.5	55 26 32	M3.0	< -4.90	< 4.0	(1)
LP 771-96	03 01 51.4	-16 35 32	M3.0	< -4.90	< 3.0	(1)
LHS 1731	05 03 20.1	-17 22 22	M3.0	< -4.90	< 2.5	(2)
G 085-041	05 07 49.2	17 58 59	M3.0	< -4.90	< 3.0	(1)
Gl 251	06 54 49.4	33 16 07	M3.0	-	< 2.5	(2)
Gl 257A	06 57 48.6	-44 17 26	M3.0	< -4.90	< 3.0	(1)
GJ 1097	07 28 45.1	-03 17 45	M3.0	-	< 2.5	(2)
LHS 1935	07 38 40.7	-21 13 25	M3.0	< -4.90	< 2.5	(2)
Gl 362	09 42 52.5	70 02 23	M3.0	-4.41	< 2.5	(2)
Gl 377	10 01 11.3	-30 23 31	M3.0	< -4.90	< 3.0	(1)
Gl 386	10 16 46.1	-11 57 36	M3.0	< -4.90	< 4.0	(1)
Gl 388	10 19 36.4	19 52 11	M3.0	-3.80	3.0	(4)
Gl 443	11 46 42.5	-14 00 43	M3.0	< -4.90	< 3.0	(1)
LTT 4562	12 11 11.9	-19 57 34	M3.0	< -4.90	< 3.0	(1)
Gl 480	12 38 53.1	11 41 47	M3.0	-	< 3.0	(3)
Gl 512A	13 28 21.0	-02 21 32	M3.0	< -4.90	< 4.0	(1)
LHS 3030	15 09 35.9	03 09 56	M3.0	< -4.90	< 4.0	(1)
Gl 581	15 19 27.5	-07 43 20	M3.0	-	< 2.5	(2)
Gl 617B	16 16 45.8	67 15 20	M3.0	< -4.90	< 2.5	(2)
Gl 655	17 07 07.6	21 33 14	M3.0	< -4.90	< 2.5	(2)
Gl 687	17 36 26.3	68 20 30	M3.0	-	< 2.5	(2)
LHS 3343	17 57 50.9	46 35 14	M3.0	< -4.90	< 4.0	(1)
LHS 462	18 18 04.1	38 46 40	M3.0	< -4.90	< 2.5	(2)
G 206-040	18 41 59.1	31 49 49	M3.0	-	< 2.5	(2)
Gl 725A	18 42 48.0	59 37 29	M3.0	-	< 2.5	(2)
Gl 735	18 55 27.3	08 24 09	M3.0	-3.91	7.7	(1)
G 207-019	19 08 29.9	32 16 53	M3.0	-	< 2.5	(2)
Gl 860A	22 28 00.3	57 41 48	M3.0	-	< 2.5	(2)
Gl 15B	00 18 23.8	44 01 35	M3.5	-	< 3.1	(5)
Gl 46	00 58 27.0	-27 51 22	M3.5	< -4.93	< 3.0	(1)
LP 771-95	03 01 51.4	-16 35 32	M3.5	-3.89	5.5	(1)
LHS 1513	03 11 33.6	-38 47 18	M3.5	< -4.93	< 3.0	(1)
GJ 1065	03 50 44.5	-06 05 30	M3.5	< -4.93	< 4.0	(1)
Gl 163	04 09 13.3	-53 22 36	M3.5	< -4.93	< 3.0	(1)
Gl 179	04 52 05.6	06 28 37	M3.5	< -4.93	< 2.5	(2)
GJ 2036B	04 53 30.8	-55 51 34	M3.5	-3.52	19.8	(1)
Steph 545A	05 06 49.6	-21 35 06	M3.5	-3.62	5.3	(1)
Gl 203	05 28 00.1	09 38 43	M3.5	< -4.93	< 4.0	(1)
G 097-052.01	05 34 15.1	10 19 15	M3.5	< -4.93	< 4.0	(1)
G 097-054	05 34 52.1	13 52 48	M3.5	< -4.93	< 2.5	(2)
LHS 1805	06 01 11.1	59 35 57	M3.5	-	< 2.5	(2)
Gl 273	07 27 30.8	05 13 12	M3.5	-	< 2.5	(2)

Table 6 — *Continued*

Name	$\alpha(J2000)$	$\delta(J2000)$	Spectral type	$\log(L_{H\alpha}/L_{bol})$	$v \sin i$ [km s ⁻¹]	ref
GI 277B	07 31 57.4	36 13 48	M3.5	-3.76	< 4.0	(1)
GJ 1105	07 58 12.5	41 18 19	M3.5	—	< 2.0	(5)
GI 317	08 40 59.5	-23 27 31	M3.5	—	< 2.5	(2)
GJ 1125	09 30 44.8	00 19 25	M3.5	—	< 2.5	(2)
LHS 2181	09 43 55.8	26 58 08	M3.5	< -4.93	< 4.0	(1)
GI 431	11 31 48.0	-41 02 52	M3.5	-3.62	20.5	(1)
GI 445	11 47 39.2	78 41 24	M3.5	—	< 2.5	(2)
LHS 2520	12 10 05.5	-15 04 10	M3.5	—	< 2.0	(5)
GI 486	12 47 57.2	09 45 09	M3.5	—	< 2.5	(2)
LHS 2651	12 55 56.5	50 55 28	M3.5	< -4.93	3.9	(6)
LHS 2784	13 42 43.2	33 17 29	M3.5	< -4.93	< 4.0	(1)
LHS 2794	13 45 50.9	-17 57 56	M3.5	< -4.93	< 2.5	(2)
GI 545	14 20 07.6	-09 37 07	M3.5	< -4.93	< 4.0	(1)
GI 553.1	14 31 01.4	-12 17 43	M3.5	—	< 2.5	(2)
GI 568A	14 53 51.9	23 33 18	M3.5	< -4.93	< 4.0	(1)
LHS 2998	14 54 27.7	35 33 03	M3.5	< -4.93	< 4.0	(1)
GI 628	16 30 18.0	-12 39 35	M3.5	—	1.5	(4)
GI 643	16 55 24.6	-08 19 27	M3.5	—	< 2.7	(5)
GJ 1207	16 57 05.4	-04 20 52	M3.5	-3.80	10.7	(1)
G 203-047	17 09 31.2	43 40 54	M3.5	< -4.93	< 4.0	(1)
LTT 15087	17 11 34.5	38 26 33	M3.5	< -4.93	< 2.5	(2)
GI 661A	17 12 07.5	45 40 09	M3.5	< -4.93	< 4.0	(1)
GI 669A	17 19 54.5	26 30 01	M3.5	-4.05	< 4.0	(1)
LHS 3295	17 29 25.9	-80 09 07	M3.5	< -4.93	< 3.0	(1)
GI 682	17 37 04.5	-44 18 57	M3.5	< -4.93	< 3.0	(1)
LHS 3333	17 50 16.0	23 45 33	M3.5	< -4.93*	< 4.5	(6)
G 205-028	18 31 58.4	40 41 06	M3.5	< -4.93	< 2.5	(2)
LP 229-17	18 34 36.5	40 07 27	M3.5	—	< 2.5	(2)
GI 725B	18 42 48.0	59 37 29	M3.5	—	< 2.5	(2)
GI 729	18 49 49.1	-23 50 08	M3.5	-3.77	4.0	(2)
GI 748	19 12 13.6	02 53 15	M3.5	—	4.6	(3)
GI 849	22 09 45.2	-04 38 11	M3.5	—	< 2.5	(2)
GI 873	22 46 50.1	44 20 05	M3.5	-3.59	3.5	(2)
GJ 1005A	00 15 27.7	-16 07 56	M4.0	< -4.94	< 3.0	(1)
GJ 1012	00 28 39.6	-06 39 44	M4.0	< -4.94	< 3.0	(1)
LP 525-39	00 32 34.7	07 29 26	M4.0	-3.54	14.7	(1)
GJ 1034	01 16 30.1	24 19 30	M4.0	< -4.94*	< 4.5	(6)
GI 82	01 59 23.2	58 31 16	M4.0	-3.52	13.8	(1)
GI 84.1B	02 05 24.3	-28 03 20	M4.0	< -4.94	< 3.0	(1)
GI 105B	02 36 14.2	06 52 06	M4.0	—	< 2.5	(2)
LHS 1426	02 37 29.9	00 21 26	M4.0	—	4.9	(6)
GI 169.1A	04 31 10.7	58 58 53	M4.0	—	< 2.0	(5)
LHS 1723	05 01 57.6	-06 56 42	M4.0	-4.51	< 3.2	(5)
LHS 5109	05 35 59.9	-07 39 00	M4.0	< -4.94	< 4.0	(1)
GI 213	05 42 08.1	12 29 33	M4.0	< -4.94	< 2.5	(2)
G 099-049	06 00 03.2	02 42 23	M4.0	-3.96	7.4	(5)
GI 300	08 12 40.8	-21 32 58	M4.0	< -4.94	< 3.0	(1)
GJ 2069B	08 31 37.5	19 23 48	M4.0	-3.85	6.5	(5)
GI 324B	08 52 41.1	28 18 59	M4.0	—	< 2.5	(2)
G 234-053	09 02 52.6	68 03 43	M4.0	< -4.94	< 4.0	(1)
GJ 1129	09 44 48.1	-18 12 47	M4.0	< -4.94	< 3.0	(1)
GI 402	10 50 52.5	06 48 34	M4.0	—	< 2.5	(2)
GJ 1148	11 41 44.4	42 44 00	M4.0	—	< 2.5	(2)
GI 447	11 47 44.0	00 48 24	M4.0	—	< 2.5	(2)
G 165-008	13 31 46.7	29 16 36	M4.0	-3.49	55.5	(5)
LHS 2836	13 59 10.9	-19 49 59	M4.0	-3.69	< 3.0	(1)
GI 555	14 34 17.0	-12 31 15	M4.0	—	< 2.5	(2)
LHS 3056	15 19 12.1	-12 45 03	M4.0	< -4.94	< 3.0	(1)
GI 592	15 36 58.8	-14 07 55	M4.0	< -4.94	< 3.0	(1)
GI 609	16 02 51.4	20 35 31	M4.0	< -4.94	< 3.0	(1)
LP 275-68	16 35 27.2	35 00 57	M4.0	-3.59	15.8	(1)
GI 699	17 57 48.1	04 43 14	M4.0	—	< 2.5	(2)
GJ 1243	19 51 09.1	46 28 57	M4.0	-3.57	22.0	(1)
GJ 1254	20 33 39.7	61 45 07	M4.0	< -4.94	< 4.0	(1)
GI 799B	20 41 50.5	-32 26 00	M4.0	-3.07	8.7	(1)
GJ 1263	21 46 39.9	00 10 19	M4.0	< -4.94	< 4.0	(1)
G 188-038	22 01 12.9	28 18 24	M4.0	-3.52	35.1	(1)
G 232-070	22 25 16.9	59 24 51	M4.0	< -4.94	< 4.0	(1)
GI 860B	22 28 00.3	57 41 48	M4.0	-4.17	4.7	(5)
GI 876	22 53 16.1	-14 15 42	M4.0	—	< 2.5	(2)
LHS 543	23 21 37.7	17 17 35	M4.0	< -4.94	< 2.5	(2)
G 190-027	23 29 22.3	41 27 51	M4.0	-3.67	14.5	(1)
GJ 1289	23 43 05.6	36 32 13	M4.0	-4.56	< 2.6	(5)
G 273-185	23 57 19.1	-12 58 40	M4.0	< -4.94	< 4.0	(1)

Table 6 — *Continued*

Name	$\alpha(J2000)$	$\delta(J2000)$	Spectral type	$\log(L_{H\alpha}/L_{bol})$	$v \sin i$ [km s ⁻¹]	ref
Gl 54.1	01 12 29.9	-17 00 01	M4.5	-4.07	< 2.5	(2)
Gl 83.1	02 00 12.3	13 03 21	M4.5	-4.16	< 2.5	(2)
G 073-045	02 20 46.1	02 58 39	M4.5	—	23.3	(6)
G 006-007	03 26 45.6	19 14 38	M4.5	—	21.9	(6)
Gl 166C	04 15 22.9	-07 39 38	M4.5	-3.95	5.5	(5)
GJ 1078	05 23 49.2	22 32 40	M4.5	—	7.2	(6)
LHS 1785	05 47 10.2	-05 12 00	M4.5	< -4.97	4.5	(6)
Gl 232	06 24 40.9	23 26 02	M4.5	—	< 3.1	(5)
Gl 234A	06 29 23.0	-02 48 45	M4.5	-3.73	5.4	(1)
LHS 1857	06 36 07.5	11 36 33	M4.5	< -4.97	4.0	(6)
LHS 1885	06 57 56.7	62 19 23	M4.5	-4.20	< 3.7	(5)
Gl 268.01	07 10 07.8	38 31 27	M4.5	-4.11	6.3	(1)
Gl 285	07 44 40.2	03 33 10	M4.5	-3.48	4.5	(4)
LHS 1950	07 51 52.6	05 33 28	M4.5	-4.97	< 2.5	(6)
Gl 299	08 11 57.2	08 46 53	M4.5	< -4.75	3.0	(5)
G 194-043	08 50 50.7	52 53 47	M4.5	—	13.1	(6)
GJ 1119	09 00 32.8	46 35 15	M4.5	-4.13	< 4.0	(1)
GJ 3542	09 17 46.0	58 25 22	M4.5	< -4.97	3.9	(6)
LHS 2206	09 53 55.4	20 56 42	M4.5	-3.93	16.5	(6)
GJ 1134	10 41 38.7	37 36 40	M4.5	< -4.97*	4.1	(6)
GJ 1138	10 49 45.8	35 32 56	M4.5	< -4.97	< 4.0	(1)
GJ 1151	11 50 58.7	48 22 44	M4.5	—	< 4.1	(5)
G 121-028	11 52 58.1	24 28 44	M4.5	< -4.97*	3.8	(6)
LHS 337	12 38 50.4	-38 22 21	M4.5	< -4.97	< 3.0	(1)
Gl 493.1	13 00 33.9	05 41 06	M4.5	-3.99	16.8	(5)
GJ 1186	14 53 40.4	11 34 25	M4.5	< -4.97	3.9	(6)
Gl 585	15 23 51.3	17 28 06	M4.5	< -4.97*	3.1	(6)
LHS 3075	15 29 43.5	42 52 53	M4.5	-4.97	< 2.5	(6)
G 180-011	15 55 31.9	35 12 00	M4.5	—	21.9	(6)
Gl 669B	17 19 53.1	26 29 59	M4.5	-3.20	6.1	(1)
GJ 1224	18 07 33.2	-15 57 46	M4.5	-3.97	< 3.0	(7)
LHS 3376	18 18 56.6	66 11 36	M4.5	-4.14	14.6	(5)
GJ 1227	18 22 28.1	62 03 10	M4.5	—	< 2.3	(5)
LHS 3459	19 22 40.9	29 26 11	M4.5	-4.97	< 4.5	(6)
GJ 1250	20 08 21.5	33 17 35	M4.5	—	15.7	(6)
Gl 791.2	20 29 47.9	09 41 18	M4.5	-3.93	32.0	(5)
Gl 799A	20 41 50.5	-32 26 00	M4.5	-3.34	13.6	(1)
GJ 1268	22 24 56.0	52 00 27	M4.5	-4.97	< 4.5	(6)
Gl 896B	23 31 51.8	19 56 14	M4.5	-3.86	24.2	(5)

References. — (1) This work (2) Browning et al. (2010); (3) Marcy & Chen (1992); (4) Reiners (2007); (5) Delfosse et al. (1998); (6) Jenkins et al. (2009); (7) Reiners & Basri (2007)

Table 7
Stars with rotation measurements from different sources. Uncertainties are discussed in Sects. 4.2 and 5.3.

Name	Spectral type	$v \sin i$ [km s ⁻¹]							
		this work	(1)	(2)	(3)	(4)	(5)	(6)	adopted
Gl 424	M0.0	—	< 2.9	—	—	—	—	< 2.5	< 2.5
Gl 678.1A	M0.0	< 4.0	—	—	—	—	—	< 2.5	< 2.5
Gl 720A	M0.0	< 4.0	—	—	< 3.0	—	—	—	< 3.0
Gl 846	M0.0	< 4.0	—	—	—	—	—	< 2.5	< 2.5
Gl 27.1	M0.5	< 3.0	—	—	—	—	—	< 3.0	< 3.0
Gl 212	M0.5	< 4.0	—	—	—	—	—	< 2.5	< 2.5
Gl 229	M0.5	< 3.0	—	—	—	1.0	—	< 2.5	1.0
Gl 369	M0.5	< 3.0	—	—	5.0	—	—	—	< 3.0
Gl 412A	M0.5	—	< 3.0	—	—	—	—	< 2.5	< 2.5
Gl 494	M0.5	10.7	—	—	—	—	—	9.7	9.7
Gl 514	M0.5	—	< 2.9	—	—	1.5	—	< 2.5	1.5
Gl 809	M0.5	—	< 2.8	—	—	—	—	< 2.5	< 2.5
Gl 2	M1.0	< 4.0	—	—	—	—	—	< 2.5	< 2.5
Gl 15A	M1.0	—	< 2.9	—	—	—	—	< 2.5	< 2.5
Gl 390	M1.0	< 3.0	—	—	—	—	—	< 2.5	< 2.5
Gl 450	M1.0	—	< 3.3	—	—	—	—	< 2.5	< 2.5
Gl 536	M1.0	< 4.0	—	—	—	—	—	< 2.5	< 2.5
Gl 570B	M1.0	—	—	—	< 3.0	—	—	< 2.5	< 2.5
Gl 649	M1.0	< 4.0	—	—	< 3.0	—	—	< 2.5	< 2.5
Gl 686	M1.0	—	< 5.0	—	—	—	—	< 2.5	< 2.5
Gl 701	M1.0	—	< 3.5	—	—	—	—	< 2.5	< 2.5
Gl 821	M1.0	< 4.0	—	—	—	—	—	< 2.5	< 2.5
Gl 908	M1.0	—	< 3.0	—	—	—	—	< 2.5	< 2.5
Gl 1	M1.5	< 3.0	—	—	—	—	—	< 2.5	< 2.5
GJ 1009	M1.5	< 3.0	—	—	—	—	—	< 2.5	< 2.5
Gl 87	M1.5	< 4.0	—	—	< 3.0	—	—	< 2.5	< 2.5
Gl 173	M1.5	< 3.0	—	—	—	—	—	< 2.5	< 2.5
Gl 205	M1.5	< 3.0	< 2.9	—	—	1.5	—	< 2.5	1.5
Gl 382	M1.5	—	< 2.9	—	—	1.8	—	< 2.5	1.8
Gl 414B	M1.5	—	—	—	< 3.2	—	—	< 2.5	< 2.5
Gl 526	M1.5	—	< 2.9	—	—	2.0	—	< 2.5	2.0
Wo 9492	M1.5	< 4.0	—	—	—	—	—	< 2.5	< 2.5
Gl 625	M1.5	—	< 3.4	—	—	—	—	< 2.5	< 2.5
Gl 667C	M1.5	< 3.0	—	—	—	—	—	< 2.5	< 2.5
Gl 745A	M1.5	—	< 3.0	—	—	—	—	< 2.5	< 2.5
Gl 806	M1.5	< 4.0	—	—	< 3.0	—	—	< 2.5	< 2.5
Gl 880	M1.5	—	< 2.8	—	—	—	—	< 2.5	< 2.5
Gl 70	M2.0	< 3.0	< 3.0	—	—	—	< 3.0	< 2.5	< 2.5
Gl 180	M2.0	< 3.0	—	—	—	—	—	< 2.5	< 2.5
Gl 226	M2.0	< 4.0	—	—	—	—	—	< 2.5	< 2.5
GJ 2066	M2.0	—	< 2.7	—	—	—	—	< 2.5	< 2.5
Gl 393	M2.0	—	< 2.9	—	—	1.5	—	< 2.5	1.5
Gl 411	M2.0	—	< 2.9	—	—	—	—	< 2.5	< 2.5
Gl 413.1	M2.0	< 3.0	—	—	—	—	—	< 2.5	< 2.5
Gl 465	M2.0	< 3.0	—	—	—	—	—	< 2.5	< 2.5
Gl 552	M2.0	—	—	—	< 3.0	—	—	< 2.5	< 2.5
Gl 569A	M2.0	< 4.0	—	—	< 3.8	—	—	< 2.5	< 2.5
Gl 745B	M2.0	—	2.8	—	—	—	—	< 2.5	< 2.5
Gl 851	M2.0	—	—	—	< 3.0	—	—	< 2.5	< 2.5
Gl 26	M2.5	< 4.0	—	—	< 3.0	—	—	< 2.5	< 2.5
Gl 408	M2.5	—	< 2.3	—	—	—	—	< 2.5	< 2.5
Gl 436	M2.5	< 4.0	—	—	< 3.0	—	—	< 2.5	< 2.5
Gl 694	M2.5	—	—	—	< 3.0	—	—	< 2.5	< 2.5
Gl 752A	M2.5	—	< 2.6	—	—	—	—	< 2.5	< 2.5
Gl 793	M2.5	—	< 3.2	—	—	—	—	< 2.5	< 2.5
Gl 48	M3.0	—	< 2.4	—	—	—	—	< 2.5	< 2.5
G 244-047.01	M3.0	< 4.0	—	3.2	—	—	—	< 2.5	< 2.5
Gl 109	M3.0	—	< 2.8	—	—	—	—	< 2.5	< 2.5
LHS 1731	M3.0	< 3.0	—	—	—	—	—	< 2.5	< 2.5
Gl 251	M3.0	—	< 2.4	—	—	—	—	< 2.5	< 2.5
LHS 1935	M3.0	< 3.0	—	—	—	—	—	< 2.5	< 2.5
Gl 362	M3.0	< 4.0	—	—	—	—	—	< 2.5	< 2.5
Gl 388	M3.0	—	6.2	—	—	3.0	3.0	2.7	3.0
Gl 581	M3.0	—	< 2.1	—	—	—	—	< 2.5	< 2.5
Gl 617B	M3.0	< 4.0	—	—	—	—	—	< 2.5	< 2.5
Gl 655	M3.0	< 4.0	—	—	—	—	—	< 2.5	< 2.5
Gl 687	M3.0	—	< 2.8	—	—	—	—	< 2.5	< 2.5
LHS 462	M3.0	< 4.0	—	—	—	—	—	< 2.5	< 2.5
Gl 725A	M3.0	—	< 2.8	—	—	—	—	< 2.5	< 2.5
Gl 860A	M3.0	—	< 3.0	—	—	—	—	< 2.5	< 2.5
Gl 179	M3.5	< 3.0	—	—	—	—	—	< 2.5	< 2.5
G 097-054	M3.5	< 4.0	—	—	—	—	—	< 2.5	< 2.5
LHS 1805	M3.5	—	< 2.7	—	—	—	—	< 2.5	< 2.5

Table 7 — *Continued*

Name	Spectral type	$v \sin i$ [km s ⁻¹]							
		this work	(1)	(2)	(3)	(4)	(5)	(6)	adopted
Gl 273	M3.5	—	< 2.4	—	—	—	—	< 2.5	< 2.5
Gl 445	M3.5	—	< 2.0	—	—	—	—	< 2.5	< 2.5
Gl 486	M3.5	—	< 2.0	—	—	—	—	< 2.5	< 2.5
LHS 2794	M3.5	< 3.0	—	—	—	—	—	< 2.5	< 2.5
Gl 628	M3.5	—	< 2.0	—	—	1.5	—	< 2.5	1.5
LTT 15087	M3.5	< 4.0	—	—	—	—	—	< 2.5	< 2.5
G 205-028	M3.5	< 4.0	—	—	—	—	—	< 2.5	< 2.5
LP 229-17	M3.5	—	< 2.0	—	—	—	—	< 2.5	< 2.5
Gl 725B	M3.5	—	< 2.8	—	—	—	—	< 2.5	< 2.5
Gl 729	M3.5	< 3.0	—	—	—	—	4.0	4.0	4.0
Gl 849	M3.5	—	< 2.4	—	—	—	—	< 2.5	< 2.5
Gl 873	M3.5	—	6.9	—	—	—	< 3.0	3.5	3.5
GJ 1005A	M4.0	< 3.0	—	—	—	—	< 3.0	—	< 3.0
Gl 105B	M4.0	—	< 2.4	—	—	—	—	< 2.5	< 2.5
Gl 213	M4.0	< 3.0	< 2.9	—	—	—	—	< 2.5	< 2.5
Gl 402	M4.0	—	< 2.3	—	—	—	—	< 2.5	< 2.5
Gl 447	M4.0	—	< 2.0	—	—	—	—	< 2.5	< 2.5
Gl 555	M4.0	—	2.7	—	—	—	—	< 2.5	< 2.5
Gl 699	M4.0	—	< 2.8	—	—	—	—	< 2.5	< 2.5
G 188-038	M4.0	35.1	29.4	—	—	—	—	—	35.1
Gl 876	M4.0	—	< 2.0	—	—	—	< 3.0	< 2.5	< 2.5
LHS 543	M4.0	< 4.0	—	—	—	—	—	< 2.5	< 2.5
Gl 54.1	M4.5	< 3.0	—	—	—	—	—	< 2.5	< 2.5
Gl 83.1	M4.5	—	3.8	—	—	—	—	< 2.5	< 2.5
Gl 234A	M4.5	5.4	6.0	—	—	—	—	—	5.4
Gl 285	M4.5	—	6.5	—	—	4.5	5.0	4.6	4.5
Gl 299	M4.5	—	3.0	—	—	—	< 3.0	—	3.0
GJ 1119	M4.5	< 4.0	—	4.0	—	—	—	—	< 4.0
GJ 1224	M4.5	—	< 5.6	—	—	—	< 3.0	—	< 3.0
GJ 1227	M4.5	—	< 2.3	—	—	—	< 3.0	—	< 2.3

References. — (1) Delfosse et al. (1998); (2) Jenkins et al. (2009); (3) Marcy & Chen (1992); (4) Reiners (2007); (5) Reiners & Basri (2007); (6) Browning et al. (2010)